ALK peptide vaccination restores the immunogenicity of ALK-rearranged non-small cell lung cancer

ALK peptide vaccination restores the immunogenicity of ALK-rearranged non-small cell lung cancer

Ines Mota, Enrico Patrucco, Cristina Mastini, Navin R. Mahadevan, Tran C. Thai, Elisa Bergaggio, Taek-Chin Cheong, Giulia Leonardi, Elif Karaca-Atabay, Marco Campisi, Teresa Poggio, Matteo Menotti, Chiara Ambrogio, Dario L. Longo, Susan Klaeger, Hasmik Keshishian, Zsófia M. Sztupinszki, Zoltan Szallasi, Derin B. Keskin, Jonathan S. Duke-Cohan, Bruce Reinhold, Steven A. Carr, Catherine J. Wu, Kelly D. Moynihan, Darrell J. Irvine, David A. Barbie, Ellis L. Reinherz, Claudia Voena, Mark M. Awad, Rafael B. Blasco & Roberto Chiarle

Abstract

Anaplastic lymphoma kinase (ALK)-rearranged non-small cell lung cancer (NSCLC) is treated with ALK tyrosine kinase inhibitors (TKIs), but the lack of activity of immune checkpoint inhibitors (ICIs) is poorly understood. Here, we identified immunogenic ALK peptides to show that ICIs induced rejection of ALK+ tumors in the flank but not in the lung. A single-peptide vaccination restored priming of ALK-specific CD8+ T cells, eradicated lung tumors in combination with ALK TKIs and prevented metastatic dissemination of tumors to the brain. The poor response of ALK+ NSCLC to ICIs was due to ineffective CD8+ T cell priming against ALK antigens and is circumvented through specific vaccination. Finally, we identified human ALK peptides displayed by HLA-A*02:01 and HLA-B*07:02 molecules. These peptides were immunogenic in HLA-transgenic mice and were recognized by CD8+ T cells from individuals with NSCLC, paving the way for the development of a clinical vaccine to treat ALK+ NSCLC.

Rearrangements in the gene encoding anaplastic lymphoma kinase (ALK) define a distinct molecular subset of non-small cell lung cancer (NSCLC) initially sensitive to ALK tyrosine kinase inhibitors (TKIs). Currently, five ALK TKIs (crizotinib, alectinib, ceritinib, brigatinib and lorlatinib)1–6 are approved for use in individuals with ALK-rearranged (ALK+) NSCLC in the United States; however, long-term disease control is limited by acquired resistance commonly mediated by secondary mutations in the ALK kinase domain, bypass track activation and other mechanisms7–10. Most individuals receiving first-line alectinib or brigatinib will experience disease progression within 3 years2,11. Resistance to subsequent treatment with lorlatinib typically occurs in less than 1 year12. Moreover, the development of central nervous system (CNS) metastasis in individuals with ALK+ NSCLC remains a clinical challenge13,14. Although immune checkpoint inhibitors (ICIs) of the programmed cell death-1 (PD-1) pathway have led to improvements in overall survival for NSCLC in general, ALK+ lung cancers in particular do not benefit from ICIs15,16. The reasons for this unresponsiveness are still poorly understood and may be due to the low tumor mutational burden of ALK+

NSCLC17,18, an unfavorable tumor microenvironment that impairs the response of tumor-infiltrating T cells19 or limited antigen presentation during ALK TKI treatment20. However, ALK protein is immunogen and elicits spontaneous immune responses when reexpressed by tumor cells21,22. Individuals with ALK+ lymphoma spontaneously develop immune responses against ALK that inversely correlate with the stage of disease, with the amount of circulating tumor cells and with cumulative incidence of relapse23–25. Also, ALK-specific tumor-reactive T cells can be detected in peripheral blood mononuclear cells (PBMCs) isolated from individuals with ALK+ lymphoma24,26. Likewise, a subset of individuals with ALK+ NSCLC has high levels of autoantibodies to ALK, which may correlate with improved survival27. Finally, vaccination with the cytoplasmic domain of the ALK protein elicits CD8+ cytotoxic T cell responses that provide long-term protection and therapeutic benefit in mouse models of ALK+ lymphoma28 and ALK+ lung cancer29. While there is evidence that the ALK protein is naturally immunogenic, human ALK peptides predicted to bind major histocompatibility complexes (MHCs)30 were not formally validated by mass spectrometry (MS) analysis nor demonstrated in tumor cells. Consequently, the mouse and human epitope sequences presented by mouse and human MHC class I molecules that engage specific T cell responses have not been precisely identified. Finally, it is unclear why the ALK-specific T cell responses are insufficient to generate effective clinical responses in individuals treated with ICIs. In this study, we sought to identify immunogenic ALK peptides in mouse models and in individuals with ALK+ NSCLC to study anti-ALK immune responses. By analyzing the spontaneous anti-ALK immune response, we demonstrated that ALK-specific CD8+ T cells spontaneously generated by ALK+ lung tumors are insufficient to achieve antitumor activity in the presence of ICIs. By contrast, we demonstrated that an ALK vaccine improved priming of ALK-specific CD8+ T cell responses, resulting in efficacious antitumor activity and control of metastatic dissemination to the CNS in combination with ALK TKIs.

Results ICIs do not increase the efficacy of ALK TKIs in lung cancer models

To study how to improve immunotherapy for ALK+ NSCLC, we leveraged two previously developed mouse models: EML4–ALK-transgenic mice that express the human EML4–ALK (E13;A20, human variant 1) rearrangement driven by the SP-C promoter29 (henceforth referred to as hEML4–ALK-transgenic mice) and BALB/c mice infected intratracheally with adenovirus carrying the CRISPR–Cas9 system to induce the Eml4–Alk rearrangement in vivo (E14;A20, mouse variant 1 (refs. 31,32); henceforth referred to as Ad-EA mice). Both models rapidly develop lung tumors that are typically detectable by imaging 12 weeks after birth in hEML4–ALK-transgenic mice or 10 weeks after adenovirus infection in Ad-EA mice, with comparable tumor morphology (Fig. 1a) 29,32. In these models, magnetic resonance imaging (MRI; Fig. 1b) allowed precise cohort stratification and tumor follow-up. Mice were divided into two cohorts and were treated with two different ALK TKIs (crizotinib or lorlatinib) alone or in combination with ICIs (anti-PD-1 or anti-PD-L1; Fig. 1c,d and Supplementary Table 1). Because ALK TKI treatment alone induces a marked reduction in tumor burden, we evaluated whether the addition of ICIs would potentiate tumor reduction at the end of treatment or delay tumor recurrence at 4 or 8 weeks after treatment suspension by quantifying the tumor volume change at each time point and comparing it to tumor volume at baseline (Fig. 1c,d and

Supplementary Table 1). At the end of treatment, lorlatinib induced almost complete regression of tumors in both hEML4–ALK-transgenic and Ad-EA mice, while crizotinib induced partial tumor regression in hEML4–ALK-transgenic mice and stabilized tumors in Ad-EA mice (Fig. 1e,h), consistent with the more potent activity of lorlatinib against ALK-driven lung cancer4 . Consequently, tumors relapsed faster in mice treated with crizotinib than in mice treated with lorlatinib (Fig. 1e–j). Anti-PD-1 or anti-PD-L1 did not induce substantial tumor reduction when administered as a monotherapy (Fig. 1e–j) and did not induce greater tumor regression at the end of treatment or delayed tumor relapse after treatment suspension when combined with ALK TKIs (Fig. 1e–j). The addition of ICIs to ALK TKIs did not increase survival in either mouse model (Extended Data Fig. 1a,b). Next, we tested whether the activity of ICIs could be observed with a higher concentration of ALK TKI that would induce a more profound tumor regression (Supplementary Table 1). Higher dosages of crizotinib induced almost complete tumor regression in hEML4–ALK-transgenic mice, as did higher dosages of lorlatinib (Extended Data Fig. 1c). Yet again, the addition of ICIs did not delay tumor relapse after treatment suspension (Extended Data Fig. 1d,e) nor did it extend mouse survival (Extended Data Fig. 1f and Supplementary Table 1). Together, these data in mouse models of ALK+ lung cancer faithfully recapitulated the absence of therapeutic benefit when ICIs are added to ALK TKIs, as observed in individuals with ALK+ NSCLC15,33.

Identification of ALK immunogenic peptides in mouse models

Despite the known immunogenicity of the ALK protein15,28,34–36, our data show that ALK+ mouse lung tumors are poorly immunogenic as they do not respond to ICIs. To directly investigate the spontaneous anti-ALK immune responses induced by ALK+ tumors, we sought to identify the ALK-specific epitopes that induce T cell responses in BALB/c mice. We therefore vaccinated mice with a DNA vaccine that encodes the cytoplasmic domain of human ALK and elicits therapeutic anti-ALK immune responses28,29. We then challenged splenocytes from vaccinated mice with a set of 21 overlapping 36-mer synthetic long peptides (SLPs) that encompass the human ALK cytoplasmic domain (Supplementary Table 2) and analyzed interferon-γ (IFNγ) production by enzyme-linked immune absorbent spot (ELISpot) assay (Extended Data Fig. 1g). SLP7 (hALK1250–1285) induced a significant increase in the number of IFNγ spots in the ALK DNA vaccine group compared to in the control group (Fig. 2a). We also observed weaker responses to the overlapping SLP20 (hALK1562–1597) and SLP21 (hALK1585–1620; Fig. 2a). In silico analysis of the immunogenic SLPs with MHC class I epitope-predicting algorithms (Supplementary Table 3) identified four ALK peptides with a high probability of binding to BALB/c mouse MHC class I; 9-mer VYRRKHQEL (hALK1058–1066), 9-mer GYQQQGLPL (hALK1585–1593) and 10-mer YGYQQQGLPL (hALK1584–1593) were predicted to bind H-2Kd , while the 9-mer PGPGRVAKI (hALK1260–1268) was predicted to bind H-2Dd (Extended Data Fig. 1h–j). To confirm the immunogenicity of these peptides and determine the type of response elicited, we vaccinated BALB/c mice with a mixture of SLPs encompassing the predicted ALK peptides and tested cytoplasmic production of IFNγ in CD4+ and CD8+ T cells stimulated with the corresponding peptides. Surprisingly, the SLPs encompassing the two 9-mer peptides and the 10-mer peptide predicted to bind H-2Kd (VYRRKHQEL, GYQQQGLPL and YGYQQQGLPL) only elicited CD4+ T cell responses

(Extended Data Fig. 2a,b). By contrast, SLP7 (hALK1250–1285) and the corresponding 9-mer PGPGRVAKI (hALK1260–1268) elicited CD8+ T cell responses exclusively (Extended Data Fig. 2a–c). To confirm that the 9-mer PGPGRVAKI directly binds H-2Dd , we edited the ALK–BALB/c-syngeneic lung cancer cell line ASB-XIV (ref. 29) to generate a cell line deficient for the Tap2 gene (ASB-XIVTAP2KO). In the absence of TAP2, peptide–MHC class I complexes are not formed, resulting in low MHC class I surface expression that can be increased after binding of an exogenous peptide, which stabilizes peptide–MHC class I complexes on the cell surface37. As expected, ASB-XIVTAP2KO cells showed low H-2Kd and H-2Dd surface expression (Extended Data Fig. 2d). H-2Dd , but not H-2Kd , was stabilized on the surface of ASB-XIVTAP2KO cells after incubation with increasing concentrations of PGPGRVAKI (Extended Data Fig. 2e), confirming its specific binding to H-2Dd . Vaccination of naive BALB/c mice with the PGPGRVAKI peptide (ALK vaccine) induced specific CD8+ T cell responses detected by IFNγ ELISpot assay (Fig. 2b) and by staining with a PGPGRVAKI–H-2Dd dextramer (ALK dextramer) in all vaccinated mice but not in control mice (Fig. 2c,d). Overall, these data identified PGPGRVAKI as an ALK immunogenic peptide that binds H-2Dd in BALB/c mice and induces specific CD8+ T cell responses. Next, we asked whether spontaneous ALK-specific CD8+ tumor-infiltrating T lymphocytes (TILs) were present in mice bearing ALK+ tumors in the lungs. ALK dextramer+ T cells represented an average of 9% of total CD8+ lung TILs in hEML4–ALK-transgenic mice but only 0.4% of CD8+ splenocytes (Fig. 2e), likely due to an intratumoral enrichment of ALK-specific CD8+ T cells caused by the presence of the ALK antigen. Yet, the presence of ALK-specific CD8+ TILs in lung tumors was not sufficient to impair tumor growth during treatment with ICIs (Fig. 1e–g). Thus, while spontaneous ALK-specific T cell responses are generated in mice with ALK+ lung tumors, they are not sufficient to achieve an effective antitumor response nor are they enhanced by ICIs.

Tumor localization determines anti-ALK immune responses

To understand why spontaneous ALK-specific CD8+ T cells are insufficient to trigger effective antitumor responses, we developed transplantable ALK+ lung tumor models by immortalizing cell lines from our mouse models. Two tumor cell lines were immortalized from Ad-EA mice (mEml4–Alk cell lines), in which EML4–ALK expression is driven by the endogenous Eml4 promoter (Extended Data Fig. 2f). These immortalized tumor cell lines (mEml4–Alk1 and mEml4–Alk2) harbored the Eml4–Alk rearrangement (Extended Data Fig. 2g), expressed the EML4–ALK fusion protein (Extended Data Fig. 2h) and showed sensitivity to all ALK Food and Drug Administration (FDA)-approved TKIs, with lorlatinib being the most effective (Extended Data Fig. 2i,j). Both exhibited comparable growth rates when injected subcutaneously in the flank of immunocompetent BALB/c and immunodeficient NOD scid gamma (NSG) mice (Extended Data Fig. 2k) and showed sensitivity to lorlatinib in vivo (Extended Data Fig. 2l). When injected intravenously into BALB/c mice, both cell lines formed lung tumors with histological features consistent with primary tumors seen in Ad-EA mice (Extended Data Fig. 3a). Therefore, these cell lines of Eml4–Alk-driven lung cancer are sensitive to ALK TKIs and can be used in immunocompetent mice to study spontaneous and induced anti-ALK immune responses. However, despite the 87% similarity of mouse and human ALK proteins38, the corresponding mouse ALK sequence differs by two amino acids from the immunogenic PGPGRVAKI peptide we identified in human ALK (Extended Data Fig. 3b). Because this difference in the amino acid sequence was predicted to reduce the affinity of the peptide for

H-2Dd (Extended Data Fig. 3b), we edited the DNA sequence of the mEml4–Alk fusion using CRISPR–Cas9 to modify the coding sequence from PGAGRIAKI to PGPGRVAKI to fully reconstitute the ALK CD8+ T cell epitope. We generated two isogenic cell lines (Eml4–AlkPGPGRVAKI-1 and Eml4– AlkPGPGRVAKI-2) that differ only by two amino acids in the ALK sequence from mEml4–Alk parental cell lines (Extended Data Fig. 3c). Like the parental mEml4–Alk cell lines, Eml4–AlkPGPGRVAKI-1 and Eml4–AlkPGPGRVAKI-2 cell lines retained sensitivity to FDA-approved ALK TKIs (Extended Data Fig. 3d,e), and phosphorylation of the EML4–ALK fusion protein was efficiently inhibited by lorlatinib (Extended Data Fig. 3f). When the cells were injected intravenously, we observed lung tumors with histologic features similar to those generated by the parental mEml4–Alk cell line (Extended Data Fig. 3g). Next, we evaluated whether mEml4–AlkPGPGRVAKI-1 and mEml4– AlkPGPGRVAKI-2 cell lines spontaneously elicited CD8+ T cell responses against the PGPGRVAKI peptide. The same number of cells (106) was injected either subcutaneously in the flank or intravenously in syngeneic BALB/c mice. Splenocytes were isolated, and ALK-specific CD8+ T cell responses were analyzed by IFNγ ELISpot assay and ALK dextramer staining. Both cell lines elicited systemic CD8+ T cell responses specific for the ALK PGPGRVAKI peptide that were absent in mice injected with the parental mEml4–Alk cell line (Extended Data Fig. 3h,i). Surprisingly, the robustness of the systemic ALK responses was significantly higher when tumors grew subcutaneously than when they were formed in the lung, as demonstrated by IFNγ ELISpot assay (Extended Data Fig. 3h) and ALK dextramer staining (Extended Data Fig. 3i). Likewise, intratumoral ALK-specific CD8+ T cell responses were higher in flank tumors than in lung tumors (Extended Data Fig. 3j). These data suggest that the amplitude of the spontaneous systemic and intratumoral ALK-specific CD8+ T cell responses is determined by localization of ALK+ tumors.

Tumor localization dictates ICI efficacy in ALK+ tumors

To determine whether these differences of ALK-specific CD8+ T cell responses translated into different antitumor activity, we treated mice Blank 1 2 3 4 5 6 7 8 9 10 11 12 13 14 15 16 17 18 19 20 21 0 100 200 a 300 b IFNγ SFU per 106 splenocytes Empty vector ALK DNA vaccine c d 0 100 200 300 400 P < 0.0001 IFNγ SFU per 106 splenocytes (PGPGRVAKI) Naive PGPGRVAKI vax 0 5 10 15 20 25 104 103 102 101 100 104 103 102 101 100 200 400 600 800 1,0K 200 400 600 800 1,0K P = 0.0005 Naive PGPGRVAKI vax Percent CD8+dextramer+ e 0 0.5 1.0 16 32 P = 0.0313 Percent CD8+dextramer+ Splenocytes TILs Naive PGPGRVAKI vax FSC 0% 20.5% FSC CD8+dextramer+ CD8+dextramer+ Fig. 2 | Identification of ALK immunogenic peptides in mouse models. a, IFNγ ELISpot assay of splenocytes isolated from mice vaccinated with an ALK DNA vaccine as schematically represented in Extended Data Fig. 1g. Data are from three technical replicates. A cutoff value of 100 IFNγ spot-forming units (SFU) was applied to provide a threshold of responsiveness. One of two independent biological experiments is shown. b, IFNγ ELISpot analysis of splenocytes isolated from naive mice and mice vaccinated with ALK short peptide 7 (PGPGRVAKI vax) with cyclic dinucleotide (CDN) adjuvant. Data are shown as average number of SFU ± s.e.m. Each dot represents one mouse (naive: n = 5 mice; vaccinated: n = 6 mice). c, Representative PGPGRVAKI-specific dextramer staining of

splenocytes from naive mice and mice vaccinated with ALK short peptide 7 (PGPGRVAKI). Cells were gated from viable CD8+ T cells. d, Quantification by dextramer staining of PGPGRVAKI-specific CD8+ T cells isolated from splenocytes of naive mice and PGPGRVAKI-vaccinated mice displayed as percent ± s.e.m. Each dot represents an individual mouse (naive: n = 10 mice; vaccinated: n = 5 mice). Data were analyzed by unpaired two-tailed Student's t-test. e, Quantification by dextramer staining of PGPGRVAKI-specific CD8+ T cells in splenocytes or lung TILs from 12-week-old hEML4–ALK-transgenic mice displayed as percent ± s.e.m. Each dot represents one mouse (n = 6 mice per group). Nature Cancer Article https://doi.org/10.1038/s43018-023-00591-2 bearing either flank or lung tumors with ICIs. When cells were injected subcutaneously into the flank, ICI treatment did not reduce tumor growth of the parental mEml4–Alk cell line lacking the PGPGRVAKI peptide (Extended Data Fig. 3k) and did not extend the overall survival of mice (Extended Data Fig. 3l), confirming the low immunogenicity of these tumors in the absence of the PGPGRVAKI peptide. By contrast, Eml4–AlkPGPGRVAKI-1 flank tumors were rejected when mice were treated with anti-CTLA-4 alone or in combination with anti-PD-1 (Fig. 3a–d), resulting in extended survival (Fig. 3e). Tumor-free mice were then rechallenged to assess ALK-specific CD8+ T cell memory responses. Rechallenged mice efficiently rejected Eml4–AlkPGPGRVAKI-1 tumor cells that were reinjected subcutaneously in the opposite flank (Fig. 3c,d) or intravenously (Fig. 3f) but did not reject mEml4–Alk tumors that lacked the PGPGRVAKI peptide. In contrast to flank tumors, ICIs were ineffective against Eml4–AlkPGPGRVAKI-1 lung tumors as measured by the number and size of lung tumors (Fig. 3g and Extended Data Fig. 4a) and overall survival (Fig. 3h). Consistently, the elicited systemic ALK-specific CD8+ T cell response from mice treated with ICIs and bearing flank tumors was higher than in mice bearing lung tumors (Fig. 3i,j). Overall, these data imply that the robustness of the spontaneous ALK-specific CD8+ T cell response depends on tumor localization and determines the response to ICIs.

ALK vaccination impairs tumor growth and prevents metastasis

Recent findings indicate that failure of response to ICIs in NSCLC might be explained by defective T cell priming induced by lung tumors compared to tumors grown in the flank39. Thus, a suboptimal priming of spontaneous ALK-specific CD8+ T cell responses by ALK+ lung tumors could explain the lack of efficacy of ICIs, suggesting that approaches aimed at improving ALK T cell priming could restore the efficacy of ICIs. Cancer vaccines targeting selected tumor antigens can revert the poor immunogenicity of some tumors by enhancing CD8+ T cell priming40–42. Therefore, we compared the spontaneous ALK-specific CD8+ T cell response elicited by ALK+ lung tumors to that elicited by the PGPGRVAKI peptide vaccine. To compare spontaneous and vaccine-induced ALK-specific T cell priming, BALB/c mice were intravenously injected with Eml4–AlkPGPGRVAKI-1 or were vaccinated with the ALK vaccine, and systemic ALK-specific CD8+ T cell responses were evaluated. CD8+ T cells from ALK-vaccinated mice demonstrated a stronger PGPGRVAKI-specific IFNγ response than CD8+ T cells primed by ALK+ lung tumors (Fig. 4a). The ALK vaccine also significantly increased the number of ALK-specific TILs compared to TILs spontaneously induced by ALK+ tumors in non-vaccinated mice (Fig. 4b), and ALK-specific TILs in vaccinated mice showed lower levels of PD-1 expression (Fig. 4c). Prompted by these findings, we evaluated the antitumor efficacy of

the ALK vaccine based on the PGPGRVAKI peptide. First, we tested the ability of the ALK vaccine alone to break tolerance in the hEML4–ALK-transgenic model that expresses the PGPGRVAKI peptide since birth. Mice were vaccinated with the PGPGRVAKI peptide, and tumor growth was followed by MRI over time (Extended Data Fig. 4b). The ALK vaccine induced a strong cytotoxic response against ALK+ cells in vivo (Extended Data Fig. 4c) and impaired tumor growth (Extended Data Fig. 4d), with responses comparable to those obtained with a DNA-based ALK vaccine29. Thus, the ALK vaccine can break tolerance and generate an effective antitumor response. Next, we tested the antitumor activity of the ALK peptide vaccine alone or in combination with anti-CTLA-4 against Eml4–AlkPGPGRVAKI-1 tumor cells growing in the lungs in the absence of ALK TKI treatment. Mice injected with Eml4–AlkPGPGRVAKI-1 tumor cells developed tumors much more rapidly than hEML4–ALK-transgenic mice. In these mice, the ALK peptide vaccine modestly extended overall survival, and the addition of anti-CTLA-4 to the ALK peptide vaccine did not yield a significant advantage (Extended Data Fig. 4e). These results prompted us to test the importance of tumor burden control by ALK TKI activity in the context of the ALK peptide vaccine. Mice injected with Eml4–AlkPGPGRVAKI-1 cells were treated with lorlatinib in combination with the ALK vaccine and/or ICIs (Fig. 4d). Treatment with lorlatinib alone extended overall survival, but all tumors relapsed after lorlatinib suspension (Fig. 4e), as we had observed in hEML4– ALK-transgenic or Ad-EA mice (Fig. 1e–j). The addition of anti-PD-1 to lorlatinib did not extend survival as in hEML4–ALK-transgenic or Ad-EA mice (Fig. 1e–j), while the addition of anti-CTLA-4 produced a modest extension of survival (Fig. 4e). By contrast, addition of the ALK vaccine to lorlatinib treatment alone or in combination with ICIs significantly extended overall survival and cured a subset of mice, with the combination of the ALK vaccine with lorlatinib and anti-CTLA-4 being the most effective (Fig. 4e). In vaccinated mice, lung tumors that were not eradicated showed increased total CD8+ TILs and ALK dextramer+ TILs compared to untreated mice or mice treated with lorlatinib alone (Extended Data Fig. 4f–h). To evaluate ALK-specific immune memory following vaccination, tumor-free mice (Fig. 4e) were rechallenged with Eml4–AlkPGPGRVAKI-1 cells more than 200 d after the last vaccination. Compared to treatment-naive mice, tumor-free mice from all vaccinated groups showed a greater expansion of systemic ALK dextramer+ CD8+ T cells after tumor rechallenge (Fig. 4f) and a significant extension of overall survival (Fig. 4g), suggesting that the ALK vaccine elicits ALK-specific CD8+ T cell memory. Finally, we evaluated the efficacy of the ALK vaccine in preventing metastatic spread of ALK+ tumors. When injected intravenously, Eml4–AlkPGPGRVAKI-1 cells not only formed lung tumors but also grew in the CNS with tropism for the meningeal space (Fig. 5a), while metastatic dissemination to other organs was not consistently detected. Remarkably, metastatic spread to the CNS was completely blocked in all vaccinated mice but not in unvaccinated mice (Fig. 5b,c). Together, these data demonstrate that increasing the robustness of anti-ALK-specific immune responses by a single-peptide vaccine in combination with ALK TKI treatment is sufficient to achieve therapeutic efficacy by extending survival, eradicating primary ALK+ lung tumors, generating ALK-specific immune memory and blocking the metastatic spread of ALK+ tumor cells to the CNS.

Tumor escape is associated with reversible MHC class I downregulation

Although significantly extending overall survival, the addition of the ALK vaccine to lorlatinib, with or without ICIs, still failed to cure a substantial portion of mice (Fig. 4e). To uncover the mechanisms of this resistance to the ALK vaccine, we isolated tumor cell lines ex vivo from each treatment group. Tumor cell lines isolated from ALK-vaccinated mice (Fig. 6a) retained the expression of the Eml4–Alk fusion transcripts and the EML4–ALK fusion protein (Extended Data Fig. 4i,j). Sequencing of Eml4–Alk mRNA demonstrated that the edited PGPGRVAKI peptide was still expressed and not mutated (Extended Data Fig. 4k), excluding loss of the antigen as a mechanism of escape. Also, surface expression of PD-L1 did not show differences among tumor lines isolated from the different treatment groups (Extended Data Fig. 5a), excluding increased PD-L1 expression as a resistance mechanism. By contrast, we observed significant downregulation of H-2Dd expression on the cell surface of ex vivo tumor cell lines isolated from vaccinated mice but not from unvaccinated mice (Fig. 6b). H-2Dd downregulation was reverted by stimulation with IFNγ (Fig. 6c) and was not associated with decreased expression of genes of the antigen presentation machinery (Lmp2, Lmp7, Tap1, Tap2, B2m, Tapbp and Mecl1; Extended Data Fig. 5b–h). To determine whether this downregulation of H-2Dd expression was sufficient to impair tumor rejection, in naive BALB/c mice, we injected tumor cell lines with high H-2Dd expression isolated from untreated mice or tumor cell lines with low H-2Dd expression isolated from ALK-vaccinated mice and treated mice with anti-CTLA-4. Anti-CTLA-4 treatment induced rejection of tumors with high H-2Dd expression (Fig. 6d,e), consistent with previous experiments (Fig. 3e), but not rejection of tumors with low H-2Dd expression (Fig. 6f,g). Further, to explore therapeutic approaches to restore H-2Dd expression, we asked whether the stimulator of IFN genes (STING) pathway, which can increase MHC class I expression in other models of lung cancer43, was also effective in ALK+ tumors cells. STING expression was not downregulated in tumor cell lines isolated ex vivo from any therapeutic group (Extended Data Fig. 5i), and all tumor lines with low H-2Dd expression isolated from ALK-vaccinated mice were sensitive to the STING agonist ADU-S100 and strongly upregulated H-2Dd expression (Fig. 6h). Thus, the reversibility of this phenotype by a STING agonist suggests a potential approach to further increase ALK vaccine efficacy by counteracting the MHC class I downregulation of tumor subclones.

Identification of immunogenic ALK peptides in individuals with NSCLC

Experiments in mice demonstrated that enhanced CD8+ T cell priming through vaccination with an immunogenic ALK peptide achieves effective antitumor responses in ALK+ lung tumors that are otherwise poorly immunogenic. To translate these findings into an ALK vaccine for individuals with ALK+ NSCLC, we sought to identify immunogenic human ALK peptides in the context of human MHC class I molecules. First, we demonstrated that most tumor cells from individuals with ALK+ NSCLC have a robust and homogenous expression of MHC class I molecules as assessed by immunohistochemistry (Fig. 7a,b). Analysis of additional cases of validated ALK+ NSCLC from Clinical Proteomic Tumor Analysis Consortium (CPTAC)44 and The Cancer Genome Atlas (TCGA) lung adenomcarcinoma (LUAD) datasets demonstrated that ALK+ NSCLC expresses HLA-A, HLA-B and HLA-C molecules at levels comparable to those observed in NSCLC driven by other oncogenes, such as mutated KRAS or EGFR (Extended Data Figs. 5j–o and 6a–f). Next, we used MS to directly identify ALK

peptides presented by human ALK+ tumor cell lines expressing HLA-A*02:01 or HLA-B*07:02 that were among the most frequent HLA alleles in a series of 100 individuals with ALK+ NSCLC treated at our institution (Supplementary Table 4). Due to the high expression of ALK in ALK+ lymphoma and its known immunogenicity in individuals with lymphoma24,30,34, we first used two ALK+ lymphoma cell lines DEL (HLA-A*02:01) and Karpas-299 (HLA-B*07:02; Supplementary Table 5). The targeted liquid chromatography–tandem MS (LC–MS/MS) analysis of eluted peptides that immunoprecipitated with HLA-A*02:01 molecules in DEL cells only yielded the AMLDLLHVA, but not the SLAMLDLLHV, peptide, even though both peptides were previously shown to be recognized by CD8+ T cells from individuals with ALK+ lymphoma30 (Extended Data Fig. 6g,h). For the HLA-B*07:02 molecule, we identified three associated ALK peptides (RPRPSQPSSL, IVRCIGVSL and VPRKNITLI) in the discovery LC–MS/MS analysis of pan-HLA immune peptidomes from Karpas-299 cells (Extended Data Fig. 7a). These ALK peptides were unequivocally assigned by the NetMHCpan4.1 algorithm to HLA-B*07:02 present in these cells (Supplementary Table 6). These same peptides were also identified in DEL and Karpas-299 cells by ultralow-flow LC data-independent acquisition MS with postacquisition targeted detection (Poisson LC–DIAMS45,46; Extended Data Figs. 6h and 7b), confirming these four as the only ALK peptides that bind HLA-A*02:01 (AMLDLLHVA) or HLA-B*07:02 (RPRPSQPSSL, IVRCIGVSL and VPRKNITLI) in ALK+ lymphoma cells (Supplementary Table 7). To translate this discovery to ALK+ lung cancer cells, we applied Poisson LC–DIAMS to MHC class I immune peptidomes isolated from the NCI-H2228 cell line that expresses the EML4–ALK fusion and both HLA-A*02:01 and HLA-B*07:02 alleles (Supplementary Table 4). A tumor biopsy of an individual with ALK+ NSCLC and the HLA-B*07:02 allele was also examined. The RPRPSQPSSL peptide was detected in NCI-H2228 cells (Fig. 7c, top), and the RPRPSQPSSL and VPRKNITLI peptides were detected in the tumor biopsy (Fig. 7c, middle and bottom). IVRCIGVSL was not detected in the tumor biopsy processed from a lysate where peptides were analyzed in the unalkylated native form (Methods). Compared to the RPRPSQPSSL precursor ion amplitude common to both NCI-H2228 and Karpas-299 cells, the absence of VPRKNITLI in NCI-H2228 cells is striking. Lack of the AMLDLLHVA peptide in NCI-H2228 cells is also noteworthy because in a reference target set of HLA-A*02:01-restricted peptides, all peptides detected in both cell lines were more abundant in the NCI-H2228 sample than in the DEL sample (Extended Data Fig. 7c). Thus, poor overall recovery of HLA-A*02:01 peptides cannot explain the absence of AMLDLLHVA in NCI-H2228 cells. Furthermore, no fusion peptides from the EML4–ALK fusion junction were predicted by NetMHCpan4.1 to bind HLA-A*02:01 or HLA-B*07:02 molecules (Supplementary Table 8). Collectively, we identified in multiple ALK+ cell lines and in an individual with ALK+ NSCLC four ALK peptides that are processed and presented by HLA-A*02:01 and HLA-B*07:02. Furthermore, a pronounced cell-specific property to the presentation of ALK peptides is observed that is not due to HLA restriction per se or simply a uniform increase or decrease in all ALK peptides (Extended Data Fig. 8a). However, when we studied the expression of critical genes involved in antigen processing and immunoproteasome activity, we could not detect significant differences at baseline between ALK+ lymphoma and lung cancer lines (Extended Data Fig. 8b–h), suggesting that other mechanisms might explain the different processing of ALK peptides in these lines. To demonstrate the potential immunogenicity of these MS-identified ALK peptides on lung and/or lymphoma-derived tumor cells, we vaccinated transgenic mice expressing either human HLA-A*02:01 or human HLA-

B*07:02 (Extended Data Fig. 9a). The AMLDLLHVA and IVRCIGVSL peptides share identical sequences in mice and humans, whereas RPRPSQPSSL differs by two amino acids (Extended Data Fig. 9b). HLA-A*02:01-transgenic mice vaccinated with two different peptides containing the core epitope AMLDLLHVA (AMLDLLHVA (AMLshort) and GGDLKSFLRETRPRPSQPSSLAMLDLLHVA (AMLlong)) developed specific CD8+ T cell responses (Extended Data Fig. 9c), consistent with a previous report30. Likewise, when we vaccinated HLA-B*07:02-transgenic mice with two different peptides containing the core epitope IVRCIGVSL or RPRPSQPSSL (IVRCIGVSL (IVRshort), FNHQNIVRCIGVSL (IVRlong), RPRPSQPSSL (RPRshort) and GGDLKSFLRETRPRPSQPSSLAM (RPRlong)), specific CD8+ T cell responses were detected in 12/12 (100%) mice vaccinated with either IVRshort peptide or IVRlong peptide and in 6/12 (50%) mice vaccinated with either RPRshort peptide or RPRlong (Fig. 7d). While no responses to the RPRPSQPSSL peptide were detected in participants, IVRCIGVSL-specific CD8+ T cell responses were detected in two of three participants with ALK+ NSCLC and in one of three participants with ALK– NSCLC after in vitro expansion of autologous antigen-presenting cell and coculture with T cells (Fig. 7e, Extended Data Fig. 9d and Supplementary Tables 9 and 10). The implications of this differential response are discussed below but provide evidence for the immunogenicity of a subset of peptides derived from the human ALK protein, consistent with their potential to serve as tumor-associated antigens for future immunotherapy-based CD8+ T cell targeting. Finally, we wanted to test the safety of the ALK peptide vaccine in our models. The expression of the endogenous ALK is low in the vast majority of normal tissues, with low expression limited to few regions in the CNS and rare intestinal neurons47, such as the hypothalamus (Extended Data Fig. 10a), which also expresses low levels of HLA-A (Extended Data Fig. 10b), HLA-B (Extended Data Fig. 10c) and HLA-C (Extended Data Fig. 10d). To study the potential toxicity of the ALK vaccine in the CNS, we vaccinated HLA-A*02:01- and HLA-B*07:02-transgenic mice with the human AMLDLLHVA and IVRCIGVSL peptides (HLA-A*02:01 and HLA-B*07:02, respectively; Fig. 8a). Both these peptides share an identical sequence within the human and mouse ALK protein (Extended Data Fig. 9b), indicating that corresponding endogenous mouse peptides might be displayed by CNS cells in the human HLA-A*02:01 and HLA-B*07:02 molecules. No differences in weight between control and vaccinated mice were observed over time (Fig. 8b). Mice did not show any motor symptoms or other behavioral changes during the period of the experiment (data not shown). HLA-A*02:01- and HLA-B*07:02-transgenic mice showed low expression of HLA molecules in the brain, as expected (Fig. 8c). Finally, HLA-A*02:01-transgenic mice vaccinated with AMLDLLHVA peptide or HLA-B*07:02-transgenic mice vaccinated with IVRCIGVSL peptide did not show a significant increase in CD8+ T cells infiltrating the hypothalamus (Fig. 8d). While these experiments lack a formal demonstration that endogenous mouse peptides are presented by human MHC class I in transgenic mice, they indicate that the ALK vaccine does not induce a T cell infiltrate in tissues with putative ALK expression, and it is not associated with obvious toxicity in mice.

Discussion

In this work, we identified immunogenic ALK peptides and tracked ALK-specific CD8+ T cell responses in mouse models of ALK+ lung tumors to demonstrate that the poor

immunogenicity of ALK+ NSCLC can be restored by enhancing the priming of ALK-specific CD8+ T cells through vaccination. Vaccination with a single ALK peptide increased the numbers of intratumoral ALK-specific CD8+ T cells, delayed tumor progression (thereby extending overall survival), appeared to cure a subset of mice when combined with ALK TKI lorlatinib treatment and prevented the metastatic spread of ALK+ tumor cells to the CNS. The lack of response of ALK+ NSCLC to ICIs is still poorly understood. ALK+ NSCLCs typically have a low tumor mutational burden48 and low levels of CD8+ TILs16, suggesting poor immunogenicity. Alternatively, ALK+ NSCLC could have an unfavorable tumor microenvironment only partially modified by ALK TKI treatment20,49. ALK itself is an immunogenic protein that induces spontaneous B and T cell responses in humans, including ALK-specific CD8+ T cell responses24,25,27. We showed that the spontaneous priming of ALK-specific CD8+ T cells is superior when tumors are localized in the flank, inducing a number of systemic and intratumoral ALK-specific CD8+ T cells that are sufficient to achieve an antitumor response with ICI treatment. By contrast, orthotopic ALK+ lung tumors induce lower numbers of ALK-specific CD8+ T cells and do not respond to ICIs. The dependency of functional T cell priming on tumor localization is also described in other mouse models and could be due to localization-dependent differences in tumor-infiltrating conventional dendritic cells (cDCs)50 or to inefficient priming in the tumor-draining lymph nodes39. Indeed, dysfunctional CD8+ T cell differentiation during T cell priming in the mediastinal lymph nodes in lung tumor-bearing mice has been recently described39, possibly due to a restraint in DC1-mediated priming of cytotoxic T cells against lung cancer51. Similar dysfunctional states of TILs have also been noted in human NSCLC52,53. In keeping with these observations, our data demonstrate that vaccination with one ALK immunogenic peptide induces stronger systemic CD8+ T cell responses than those spontaneously elicited by ALK+ lung tumors, resulting in higher intratumoral CD8+ T cell infiltration and superior therapeutic activity, suggesting that the unresponsiveness to ICIs of ALK+ lung tumors might be due to an insufficient or dysfunctional priming against the ALK antigen. Importantly, the ALK vaccine can break tolerance as demonstrated by the immune responses obtained in hEML4–ALK-transgenic mice that express the PGPGRVAKI peptide since birth and by HLA-transgenic mice vaccinated with the AMLDLLHVA or IVRCIGVSL peptides that share an identical sequence in human and mouse ALK, indicating that vaccination with a potent ALK vaccine should be able to overcome tolerance in humans. We observed superior antitumoral activity of anti-CTLA-4 compared to anti-PD-1 not only when administered as monotherapy against subcutaneous tumors but also in combination with the ALK vaccine against lung tumors. Anti-CTLA-4 treatment also helped to generate a stronger ALK-specific CD8+ T cell memory response that protected mice when rechallenged with tumors cells growing in the flank or systemically. Likewise, the ALK-specific CD8+ T cell memory response was stronger in tumor-free mice that were vaccinated together with anti-CTLA-4 treatment. These data are consistent with the role of CTLA-4 in regulating T cell priming54,55. Anti-CTLA-4 treatment is also known to deplete CD4+ regulatory T (Treg) cells in mice56; however, EML4–ALK lung tumors in mice are infiltrated by only a few CD4+ Treg cells29, and the PGPGRVAKI peptide selectively elicits CD8+ T cell responses, suggesting that the superior efficacy obtained by combination with anti-CTLA-4 treatment is more likely due to enhanced priming than depletion of Treg cells. Up to 40% of individuals with ALK+ NSCLC may develop CNS metastases that respond well to second- and third-generation ALK TKIs but nonetheless

indicate a poor prognosis13,14, and interventions to control intracranial disease are critical to extend survival14. We showed that ALK vaccination, but not the spontaneous immunogenicity of lung tumors, induced an ALK-specific immune response that completely prevented the metastatic spread of ALK+ tumor cells to the brain. The prevention of metastatic spread was complete in all mice treated with a combination of ALK TKIs and the ALK vaccine with any ICI therapy. However, it remains to be seen whether the ALK vaccine will also be effective against established brain lesions in combination with ALK TKIs. Loss of MHC class I molecules is one mechanism of immune evasion in which the presentation of specific antigens by tumor cells is reduced or lost. Focal HLA allele loss of heterozygosity occurs in up to 40% of NSCLC cases57, while selective loss of an HLA allele can be observed as a direct mechanism of tumor immune evasion against specific peptides58. In our models, the ALK protein was not lost in tumors that escaped after treatment with ALK TKIs and the ALK vaccine, in line with the strong dependency on the ALK oncogenic activity of ALK+ NSCLC. By contrast, we observed downregulation of the expression of MHC class I molecules. Importantly, MHC class I downregulation was reversible in vitro after treatment with recombinant IFNγ or STING agonist, suggesting that a combination treatment with STING agonists59 during or after ALK vaccination could further delay immune evasion by restoring MHC class I expression and the presentation of ALK antigens. Based on our preclinical findings, the development of a clinical therapeutic ALK vaccine is an attractive approach. We showed that different formulations of the ALK vaccine (DNA, naked peptides with CDN adjuvant and amphiphilic peptides with amph-CpG adjuvant) induced comparable immune responses. ALK vaccines based on DNA or RNA encoding the entire cytoplasmic domain might be associated with risks of secondary integration in the genome, which might represent a safety concern due to the oncogenic potential of the cytoplasmic domain of the ALK protein. By contrast, a peptide-based vaccine or an RNA-based vaccine encoding short ALK peptides might eliminate the risks associated with a possible ALK integration. The safety of the ALK vaccine will require testing in a clinical trial. Although the ALK vaccine was safe with ALK TKIs and ICIs in our mouse models, the tolerability and efficacy of an ALK vaccine in combination with other therapies will need to be prospectively evaluated in human clinical trials. MHC class I expression is conserved in ALK+ NSCLC, and ALK expression is typically preserved in tumors that become resistant to ALK TKIs9 , which suggests that ALK vaccination could be an approach to enhance immunotherapy against ALK+ NSCLCs that develop resistance to ALK TKIs. We identified ALK immunogenic peptides in the context of two frequent HLA molecules (HLA-A*02:01 and HLA-B*07:02) presented by ALK+ lymphoma cells, ALK+ lung cancer lines and a human tumor biopsy. Interestingly, despite the high sensitivity of Poisson LC– DIAMS, the AMLDLLHVA peptide was clearly identified in HLA-A*02:01 ALK+ lymphoma cells but not in NSCLC cells. Likewise, while three HLA-B*07:02 ALK peptides were readily identified in ALK+ lymphoma cells, only two of these ALK peptides were identified in the tumor biopsy and one in the NCI-H2228 cell line. These differences could reflect a sensitivity issue due to the abundance and localization of ALK protein; alternatively, the processing of the ALK peptides in different tumor types could reflect cell-specific or fusion-specific mechanisms. In ALK+ lymphoma cells, the NPM–ALK fusion is abundantly expressed in the cytoplasm and in the nucleus of tumor cells, while in lung cancer, the EML4–ALK fusion is less abundant and is localized to the cytoplasm. Further, it remains to be investigated whether different EML4–ALK variants or ALK fusions with different partners might display different processing of ALK peptides. Cell-specific antigen

processing has been observed in other tumors45 and could have implications for tailoring the formulation of the ALK vaccine to the tumor type to be targeted. While some variability in the processing of ALK peptides between different tumors might well exist, the identification of immunogenic human ALK peptides in the current study paves the way for the clinical development of an ALK vaccine that could be used to broadly target ALK-driven tumors in individuals with selected HLAs and could facilitate the development of alternative immunotherapies, such as the transfer of T cells redirected by engineered T cell antigen receptors to recognize these ALK peptides60.

Methods

Participants and sample collection

Individuals with NSCLC at the Dana–Farber Cancer Institute (DFCI) consented to an institutional review board-approved correlative research protocol that allowed for review of medical records and sample collection. Lung cancer mutation status was determined using standard Clinical Laboratory Improvement Amendments-certified clinical assays in the Center for Advanced Molecular Diagnostics at Brigham and Women's Hospital. For each participant, 10 ml of whole blood was collected into K3-EDTA tubes, and PBMCs were isolated by Ficoll-Paque Plus density separation (GE Healthcare) and thereafter frozen until use.

Human and mouse cell lines

Human ALK+ NSCLC cell lines (inv(2)(p21;p23), NCI-H3122, variant 1, E13;A20 (https://www.cellosaurus.org/CVCL_5160), NCI-H2228 (https://www.cellosaurus.org/CVCL_1543), CRL-5935, variant 3, E6;A20) were obtained from DFCI. Human ALK+ anaplastic large cell lymphoma cell lines (DEL and Karpas-299) were obtained from DSMZ German cell collection; the mouse ASB-XIV cell line derived from BALB/c mice was purchased from Cell Lines Service (400120), and the mouse KP1233 lung cancer cell line (immortalized from C57BL/6 KRASG12D mice) was kindly gifted by T. Jacks (Koch Institute). HEK-293FT packaging cells were used for lentivirus production and were obtained from Thermo Fisher (R70007). The NIH-3T3-hCD40Ligand cell line was kindly gifted by G. Freeman (DFCI). All cell lines were passaged for less than 6 months after receipt and resuscitation and were maintained either in DMEM (Lonza; NCI-H3122, NCI-H2228, ASB-XIV, KP1233 and HEK-293FT cell lines) or in RPMI (Lonza; DEL and Karpas-299 cell lines) with 10% fetal bovine serum (FBS; Gibco), 2% penicillin, 5 mg ml–1 streptomycin (Gibco) and 1% glutamine (Gibco) and were grown at 37 °C in a humidified atmosphere with 5% CO2. NIH-3T3-hCD40L cells were cultivated in DMEM/F12 HEPES (Gibco), 10% FBS, 15 µg ml–1 gentamycin (Gibco) and 200 µg ml–1 G418 (Gibco). All cell lines were monitored for Mycoplasma by IDEXX BioAnalytics (Impact III PCR profile). Generation of Eml4–Alk mouse cell lines The immortalized mouse cell lines mEml4–Alk1 and mEml4–Alk2 were obtained from BALB/c Tp53-knockout mice infected with adenovirus carrying the CRISPR–Cas9 system (single guide RNA (sgRNA) Eml4 and sgRNA Alk) as previously described31,32. Primary cultures were established using a lung dissociation kit (Miltenyi Biotec) according to the manufacturer's instructions and were cultured primarily in three-dimensional culture and finally in two-dimensional culture. The immortalized humanized mouse cell lines Eml4–AlkPGPGRVAKI-1 and Eml4– AlkPGPGRVAKI-2 were derived from mEml4–Alk1 . To avoid Cas9

off-targets, electroporation of short-lifetime recombinant Cas9 protein was performed. Recombinant Cas9 protein was mixed with trans-activating CRISPR RNA and CRISPR RNA (TTGCTATTCTTCCAGCTCCT; IDT) to generate ribonucleoproteins. Ribonucleoproteins were then transfected by electroporation into mEml4–Alk1 cells together with the single-stranded oligodeoxynucleotides (TATGAAATTAAGAACCCTGTTTTCTTCCCAGGGATATTGCTGCTAGAAACTGTCTGTTGACCTGCCCAGGTCCGGGAAGAGTAGCAAAGATTGGAGACTTTGGGATGGCCCGAGATATCTA; IDT) carrying the edited sequence using the SE Cell Line 4D-Nucleofector X kit S (Lonza) and the program CM-137. After electroporation, Scr7 (100 nM, Sigma) was used to inhibit non-homologous end joining and favor homologous recombination. Once recovered from electroporation, single-cell clones were generated through consecutive dilutions and validated through DNA and RNA sequencing.

Generation of ex vivo cell lines from lung tumors

Mouse lung lobules were collected, and individual lung tumors were isolated and mechanically disaggregated until a single-cell suspension was obtained. Cells were plated in six-well plates consecutively in DMEM complete medium. After 15 d in culture and at least three passages, ex vivo cell lines were established. All mouse cell lines were further tested for the presence of the mouse and human EML4–ALK rearrangement and passaged for less than 6 months after primary culture. Cells were maintained in DMEM (Lonza) with 10% FBS (Gibco), 2% penicillin, 5 mg ml–1 streptomycin (Gibco), 1% glutamine (Gibco), 1 mM sodium pyruvate (Gibco) and 0.5 mM non-essential amino acids (Gibco) and were grown at 37 °C in a humidified atmosphere and 5% CO2. All cell lines were monitored for Mycoplasma by IDEXX BioAnalytics (Impact III PCR profile).

Prediction of ALK peptide binding to mouse MHC class I

NetMHCpan4.1 (ref. 61) and NetMHC4.0 (ref. 62) algorithms (https://services.healthtech.dtu.dk/service.php?NetMHCpan-4.1 and https://services.healthtech.dtu.dk/service.php?NetMHC-4.0) were used to predict MHC class I (H-2Kd and H-2Dd) binding for all possible 8- to 11-amino acid-long sequences corresponding to ALK peptides. Predicted MHC class I binders were selected based on their relative ranking in NetMHCpan4.1 (the top 0.5% of ranked peptides were considered strong binders).

Mice

Mouse strains used include transgenic SP-C-EML4–ALK and NPM–ALK expressing the hEML4–ALK fusion (hEML4–ALK-transgenic mice) or NPM–ALK fusion, respectively, as previously described29. BALB/c mice were purchased from Charles River. CB6F1-B2mtm1Unc Tg(B2m)55Hpl Tg(HLA-B*0702/H-2Kb)B7 mice (HLA-B*07:02-transgenic mice) were purchased from Taconic. NSG and B6.Cg-Immp2lTg(HLA-A/H2-D)2En ge/J mice (HLA-A*02:01-transgenic mice) were purchased from Jackson Laboratory). Ad-EA mice were generated by using the CRISPR–Cas9 system to induce Alk rearrangements in vivo, as previously described32. Mice were housed in our specific pathogen-free animal facilities. In all in vivo experiments, 8- to 12-week-old females were used, and all studies were performed in

accordance with procedures approved by either University of Turin or the ARCH-accredited Animal Studies Committee of Boston Children's Hospital, Harvard Medical School. Regarding subcutaneous tumor volume, the humane endpoint was reached when tumors were 1.5 cm or greater in diameter. Maximum tumor size was not exceeded.

MRI

Anatomical T2-weighted coronal images were acquired with a respiratory-triggered multislice fast spin echo RARE sequence (repetition time = 4 s, echo time = 4.5 ms, rare factor = 16, field of view = 30 mm2 , matrix = 256 × 256, slices = 16–20, slice thickness = 1 mm and two averages, providing an in-plane spatial resolution of 117 μm) with a 7T MRI (Bruker Avance III) scanner equipped with a quadrature 1H coil. Animals were anesthetized by intraperitoneal injection of a combination of Rompun (Bayer; 5 mg per kg (body weight)) and Zoletil 100 (Laboratoires Virbac; 20 mg per kg (body weight)); breathing was monitored during acquisition of the MR images with a respiratory sensor (SA Instruments). Tumor volumes and numbers of masses calculations were performed by manual segmentation (slice-by-slice contouring) with ITK-SNAP software (www.itksnap.org).

ALK inhibitors

Crizotinib and lorlatinib were kindly gifted by Pfizer. Alectinib, ceritinib and brigatinib were purchased from Selleckchem. For in vivo treatment, crizotinib and lorlatinib were administrated via oral gavage either once a day (DIE) or twice a day (BID) as indicated. Crizotinib was administrated for short-term treatment (15 d), and lorlatinib treatment was performed either in the short term (15 d) or prolonged treatment (4 or 8 weeks) as indicated. Crizotinib was administered either at 40 mg per kg (body weight) BID or at a higher dose (100 mg per kg (body weight) DIE). Lorlatinib was administered either at 2 mg per kg (body weight) BID or at a higher dose (10 mg per kg (body weight) DIE). The vehicle solution was 0.5% methylcellulose (Sigma-Aldrich) and 0.05% Tween-80 (Sigma-Aldrich).

ICIs

When using transgenic NSCLC mouse models, mice were treated intraperitoneally with 300 μg or 200 μg of anti-PD-1 (clone RMP1-14, Bioxcell) and anti-PD-L1 (clone 10F.9G2, Bioxcell) and control anti-rat polyclonal IgG, administrated alone or in combination with ALK inhibitors (either crizotinib or lorlatinib) every 3 d or every week for a total of five injections. Syngeneic mouse models transplanted with tumor cells were treated intraperitoneally with 200 μg of anti-PD-1 and/or anti-CTLA-4 (clone 9D9, Bioxcell) on days 3, 6 and 9 after tumor transplantation (three injections per mouse). When combined with the ALK inhibitor lorlatinib and/or vaccination, intraperitoneal injections were performed at day 6 after tumor injection and were synchronized with lorlatinib treatment.

DNA and peptide ALK vaccination

ALK DNA vaccination was used for ALK peptide screening and was performed as previously described29. Briefly, 50 μg of control pDEST (Invitrogen) or pDEST-ALK vectors was diluted in 20 μl of 0.9% NaCl with 6 mg ml–1 polyglutamate and injected on days 1 and 7 into both tibial muscles of anesthetized BALB/c mice. Electric pulses were applied through two electrodes placed on the skin; two square-wave 25-ms, 375 V cm–1 pulses were generated by a T820

electroporator (BTX)29. ALK peptides were purchased from Genscript. The peptide vaccine was prepared by mixing the corresponding peptide (10 μg) with CDN adjuvant (25 μg), according to manufacturer's instructions. Mice were vaccinated subcutaneously with 100 μl of peptide vaccine. For amph vaccination (Extended Data Fig. 4d), the hALK1260–1268 peptide and CpG adjuvant were both modified with an amphiphilic tail as previously described63. Twenty micrograms of amph peptides was mixed with 1.24 nmol of amph-CpG and administered subcutaneously in the base of the tail.

In vivo cytotoxicity assay

In vivo cytotoxicity assays were performed as previously described29. Briefly, vehicle-vaccinated and ALK-vaccinated mice (both peptide and ALK DNA-vaccinated mice) were injected intravenously with 1 × 107 wild-type splenocytes mixed with 1 × 107 NPM–ALK-transgenic splenocytes labeled with different concentrations of carboxyfluorescein succinimidyl ester (CFSE; 0.5 μM and 5 μM, respectively). After 72 h, CFSE+ CD4+ splenocytes were stained with TRITC-labeled anti-CD4 and analyzed by flow cytometry. ALK-directed specific cytotoxicity was calculated as the decrease in ALK+ CD4+ T cells (CFSEhigh) after normalization with the total number of CD4+ CFSE+ T cells.

Tumor grafting

For syngeneic subcutaneous tumor transplantation, a total of 1 × 106 immortalized mouse cells were subcutaneously inoculated into the right dorsal flanks of 8- to 12-week-old BALB/c mice in 100 μl of PBS. Subcutaneous tumor-bearing mice were randomized and grouped into different treatment groups when tumors reached 5 mm in diameter. Tumor volume was measured by caliper measurements every 3 d in a blinded fashion and was calculated according to the following equation: H × W2/2. In accordance with our mouse protocol, maximal tumor diameter was 15 mm (humane endpoint) in one direction, dictating the end of the experiment. For the orthotopic syngeneic mouse model, a total of 106 immortalized mouse cells were inoculated intravenously into the tail veins of 8- to 12-week-old BALB/c mice in 100 μl of PBS. Mice were randomized into different treatment groups. In accordance with our mouse protocol, the humane endpoint was reached when mice showed difficulty breathing, lost locomotor activity, lost body weight and/or presented an abnormal coat condition or posture. For the rechallenge study, mice were injected either subcutaneously in the opposite flank or intravenously with 106 immortalized mouse cells in 100 μl of PBS and were monitored as described above

Tissue collection, immunohistochemistry and metastasis assay

For histologic evaluation, lung lobules were collected, fixed in formalin and embedded in paraffin as previously described29. CD8+ T cells were quantified by high-power field by measuring the number of CD8+ T cells among the total number of tumor cells. Immunohistochemistry for mouse CD8a was performed with anti-CD8 (Cell Signaling Technology, clone D4W2Z, 98941). For flow cytometry and/or ex vivo experiments, both subcutaneous tumor and lung lobules were collected and either mechanically disaggregated or dissociated into mouse tumor cell suspensions using a mouse tumor disassociation kit 651

(130-096- 730, Miltenyi Biotec), according to the manufacturer's protocol. After red blood cell lysis and filtration, cell suspensions were stained for live/dead cells with Zombie Aqua (Zombie Aqua BV510, Biolegend, 423101/423102) and were subjected to flow cytometry. Total blood was collected from the venous sinus into a BD Vacutainer 2-ml blood collection tube with K3-EDTA. For the metastatic assay, brains were collected, fixed in formalin and embedded in paraffin, and several tissue sections were stained for H&E and analyzed for micrometastases. For brain toxicity analysis, brains from HLA-A*02:01- and HLA-B*07:02-transgenic mice were collected after the vaccination protocol, fixed in formalin and embedded in paraffin, and several tissue transverse sections were stained for H&E, human pan-HLA with a mouse monoclonal antibody to HLA class I ABC (clone EMR8-5, Abcam, ab70328) and mouse CD8+ T cells and were analyzed for CD8+ T cell infiltration in the hypothalamus region.

ELISpot assay

The IFNγ release ELISpot assay was performed using a commercial kit (mouse IFNγ ELISpot, Mabtech) according to the manufacturer's instructions. Briefly, the ELISpot plate was prepared under sterile conditions and washed with sterile PBS (200 µl per well) five times. Consecutively, the plate was conditioned with fresh DMEM (200 µl per well containing 10% of the same FBS used for the splenocyte suspensions and incubated for 30 min at room temperature. After incubation, the medium was discarded, and 2.5 × 105 splenocytes were plated in each well together with the appropriate stimuli. The plate was incubated overnight at 37 °C in a humidified chamber with 5% CO2. The day after, cells were discarded, and the plate was washed five times with PBS. Biotinylated detection of monoclonal antibody to IFNγ (1 µg ml–1) was added into the wells, followed by 2 h of incubation at room temperature. Successively, and after another wash step, the plate was incubated for an additional 1 h at room temperature with diluted streptavidin–ALP (1:1,000) in PBS and 0.5% fetal calf serum at 100 µl per well. Finally, the plate was washed again five times with PBS, followed by the addition of substrate solution BCIP/NBT-plus. Tap water was used to stop the reaction when distinct spots appeared. All plates were evaluated by a computer-assisted ELISpot reader (CTL Immunospot analyzer).

Intracellular cytokine staining

Mice were bled, and 100–200 µl of peripheral blood was lysed with red blood cell ACK lysis buffer. PBMCs were plated in U-bottom, 96-well plates with T cell medium (RPMI, 10% FBS, penicillin/streptomycin, glutamine and HEPES 15 mM) and pulsed with 10 nmol of individual peptides. After 2 h, Brefeldin A was added (BD Cyotfix/Cytoperm plus kit, BD Pharmigen) and incubated for 4 h. PBMCs were then washed with fluorescence-activated cell sorting (FACS) buffer and incubated with Fc blocker (1:100; CD16/CD32 mouse Fc block, BD Pharmigen) for 10 min at room temperature before staining with PE-CD4 (1:100; clone GK1.5, Miltenyi) and FITC–CD8 (1:100; clone 53-6.7, Miltenyi) at 4 °C for 20 min. After washing with FACS buffer, cells were fixed with BD Cytofix/Cytoperm fixation solution for 20 min at 4 °C and washed with BD Perm Wash buffer (BD Cytofix/Cytoperm plus kit, BD Pharmigen) before incubating with allophycocyanin (APC)–anti-IFNγ (1:50 in BD Perm Wash buffer, BD Pharmigen) for 30 min at

4 °C. Cells were analyzed by flow cytometry once washed with BD Perm Wash Buffer and FACS buffer consecutively.

Dextramer staining and flow cytometry

APC-conjugated H-2Dd –PGPGRVAKI dextramer reagents were obtained from Immudex. Briefly, 1 × 106 cells (either from total splenocytes or total subcutaneous tumor and/or lung disaggregation) were stained with Zombie Aqua (Biolegend) viability marker for 30 min at room temperature. After this initial step, cells were treated with 50 nM dasatinib at room temperature for 30 min. Dextramer staining was performed together with mouse Fc block for 20 min at room temperature protected from light. Without prior washing, cells were stained with mouse FITC–CD8-conjugated (clone G42-8, BD Pharmingen) antibody for 10 min at 4 °C. After washing, cells were ready to be acquired. When referred, PD-1 (clone RMP1-30, BV421-PD-1, BD Pharmingen) expression was also evaluated together with dextramer staining added together with FITC–CD8. H-2Dd expression was measured on relapsed tumors after treatment. Tumor lungs were isolated and cultured ex vivo until primary cultures were established. Briefly, cells seeded in complete DMEM were detached by using cold PBS. Resuspended cells were then stained with APC–anti-H-2Dd (clone 34-1-2S, Thermo Fisher) for 20 min, washed and resuspended again in PBS. All cells were acquired on a BD Celesta flow cytometer (BD Bioscience) and analyzed by using FlowJo software (FlowJo).

Compounds and treatments

Recombinant IFNγ (mouse IFNγ, 794 485-MI) was purchased from R&D Systems 795 and reconstituted in 1% bovine serum albumin. For experiments to engage STING, cells were treated with ADU-S100 (50 μM; CT-ADUS100, ChemieTek) for 24 h. Flow cytometry analysis of H-2Dd surface expression was performed as a readout for both experiments as described above (PE–H-2Dd , clone 34-2-12, BD Pharmigen).

Peptide binding assay

To knock out the Tap2 gene in the ASB-XIV cell line, we used CRISPR– Cas9 technology with sgRNAs (ATAGAGGGCACCCTGCGACT or GAGCACCTCAGTAGTCCGAG) targeting Tap2 exon II that were cloned into lentiCRISPR v2 (Addgene, 52961). After lentiviral infection and puromycin selection, single-cell clones were obtained through consecutive dilutions, and expression of H-2Dd and H-2Kd was analyzed by flow cytometry (PE–H-2Dd , clone 34-2-12, BD Pharmigen; PE–H-2Kd , clone SF1-1.1, BD Pharmigen) to evaluate the downregulation of MHC class I. The H-2Kd -associated peptide FYIQMCTEL (IEDB, epitope 18405) was used to validate the ASB-XIV-TAP2KO tool in a binding assay before evaluating PGPGRVAKI binding. Briefly, cells were incubated with different concentrations of peptide at 26 °C for 16 h and then at 37 °C for 3 h. Cells were then washed, detached with 2 mM EDTA, stained and analyzed for H-2Dd and H-2Kd surface expression by flow cytometry.

Cell lysis and immunoblotting

Cells were lysed in GST buffer (10 mM MgCl2, 150 mM NaCl, 1% NP-40, 2% glycerol, 1 mM EDTA and 25 mM HEPES, pH 7.5) with protease inhibitors (1 mM phenylmethylsulfonyl fluoride, 10 mM NaF, 1 mM Na3VO4 and protease inhibitor cocktail (Amresco)). The following

antibodies were used: anti-pALK (Y1586; Cell Signaling Technology), anti-ALK SP8 16670 (Abcam) and anti-actin (Sigma).

DNA and RNA extraction, PCR, quantitative real-time PCR and Sanger sequencing

DNA and RNA were extracted as previously described29. PCR reactions were established to detect both genomic DNA and cDNA of peptide 7. PCR products were purified using the QIAquickPCR purification kit (QIAGEN), and the amplicons were sequenced by GeneScript. Sanger sequencing data were analyzed with SnapGen software (SnapGen). The following primers were used: ALK peptide 7 gDNA forward (TATGAAGGCCAGGTGTCTGGAATGC) and reverse (GACAAACTCCAGAACTTCCTGGTTGC) and ALK peptide 7 cDNA forward (ACCTCGACCATCATGACCGACT) and reverse (ACACCTGGCCTTCATACACCTC). Quantitative real-time PCR was performed using Power SYBR Green PCR master mix (Applied Biosystems), according to the manufacturer's instructions. Relative gene expression was measured for the mouse genes Alk, Lmp2, Lmp7, Mecl1, Tap1, Tap2, B2m, Tapbp and Sting by using the following primers: Alk forward (GCTGGACCTTCTGCATGTGGC) and reverse (AGGCTTCAGGGGGCATCCAC), Lmp2 forward (CATGAACCGAGATGGCTCTAGT) and reverse (TCATCGTAGAATTTTGGCAGCTC), Lmp7 forward (ATGGCGTTACTGGATCTGTGC) and reverse (CGCGGAGAAACTGTAGTGTCC), Mecl1 forward (CTTTACTGCCCTTGGCTCTG) and reverse (GTGATCACACAGGCATCCAC), Tap1 forward (GGACTTGCCTTGTTCCGAGAG) and reverse (GCTGCCACATAACTGATAGCGA), Tap2 forward (CTGGCGGACATGGCTTTACTT) and reverse (CTCCCACTTTTAGCAGTCCCC), B2m forward (TTCTGGTGCTTGTCTCACTGA) and reverse (CAGTATGTTCGGCTTCCCATTC), Tapbp forward (GGCCTGTCTAAGAAACCTGCC) and reverse (CCACCTTGAAGTATAGCTTTGGG) and Sting forward (GGTCACCGCTCCAAATATGTA) and reverse (GGTCACCGCTCCAAATATGTA). Relative gene expression was measured for the human genes TAP1, TAP2, B2M, TAPBP, LMP2 and LMP7 by using the following primers: TAP1 forward (TGGACGCGGCTTTACTGTG) and reverse (CACCTGCGTTTTCGCTCTTG), TAP2 forward (TGCCCCGCATATTCTCCCT) and reverse (GCAGCCCTCTTAGCTTTAGCA), B2M forward (GAGGCTATCCAGCGTACTCCA) and reverse (CGGCAGGCATACTCATCTTTT), TAPBP forward (TGGACCGGAAATGGGACCT) and reverse (CCCCAGAAGGGTAGAAGTGG), LMP2 forward (GCACCAACCGGGGACTTAC) and reverse (CACTCGGGAATCAGAACCCAT) and LMP7 forward CACGCTCGCCTTCAAGTTC and reverse AGGCACTAATGTAGGACCCAG.

Cell viability assay

Cell viability assays were performed in all immortalized mouse cell lines by using CellTiter-Glo (Promega) according to the manufacturer's instructions. Briefly, cells were seeded into white-walled 96-well plates (three wells per sample) in DMEM and incubated using a ten-point dose titration scheme of ALK inhibitors (crizotinib, lorlatinib, alectinib, ceritinib and brigatinib) from 1 nM to 1 μM. After 72 h, CellTiter-Glo reagent was added to each well, and luminescence output data were taken by a GloMax-Multi detection system (Promega). The corresponding half-maximal inhibitory concentration value for each ALK inhibitor was calculated with GraphPad Prism 9 software (GraphPad).

DC generation

Frozen PBMCs from individuals with NSCLC were thawed, resuspended in cold RPMI containing 3% human AB heat-inactivated serum (Sigma-Aldrich) and cultured in a T-175

culture flask for 50 min at 37 °C and 5% CO2 to induce the attachment of CD14+ monocytes to the plastic. The remaining floating PBMCs were removed with gentle washes of PBS and warm medium. Monocytes were then cultured in RPMI containing 3% human AB heat-inactivated serum, 2% penicillin/streptomycin, 1% glutamine and 25 nM HEPES with granulocyte– macrophage colony-stimulating factor (120 ng ml–1; Preprotech) and interleukin-4 (IL-4; 70 ng ml–1; Preprotech). Fresh granulocyte–macrophage colony-stimulating factor and IL-4 were added on days 3 and 5. On day 6, poly(I:C) (30 µg ml–1; Sigma-Aldrich) was added for 24 h to induce DC maturation.

B cell activation and expansion

B cells were expanded using the CD40 system64,65. Briefly, NIH3T3-CD40L cells were irradiated (96 Gy) and plated in a six-well plate (400,000 cells per well) without gentamycin. The following day, 8 × 106 PBMCs were resuspended in 4 ml of IMDM (glutamine, HEPES; Gibco) containing 10% human heat-inactivated AB serum (Sigma-Aldrich), transferrin (50 µg ml–1; Lonza), insulin (5 µg ml–1; BioXtra), cyclosporine A (5.5 × 10–7 M; Sigma-Aldrich), IL-4 (2 ng ml–1; Preprotech) and gentamycin (15 µg ml–1; Gibco) and cocultured with irradiated NIH-3T3-CD40L cells for 5 d. PBMCs were then counted and cultured at the same concentration together with newly irradiated NIH-3T3-CD40L cells for an additional 3 d. After 12 d, 95% of the cells were CD19+ and could be expanded similarly every 3–4 d at a concentration of 106 cells per ml. B cells were always used after 15 d of culture.

Generation and expansion of ALK-specific CD8+ T cells

CD8+ T cells were purified using magnetic beads (CD8+ T cell isolation kit, Miltenyi) and cocultured with DCs (20:1; around 106 CD8+ T cells:50,000 DCs) in AIM V medium (Gibco) with 5% human AB heat-inactivated serum (Sigma-Aldrich), 20 U ml–1 IL-2 (Peprotech) and 10 ng ml–1 IL-7 (Peprotech). Before coculture, DCs were pulsed with 10 µg ml–1 of the desired peptide in AIM V medium without serum at 37 °C and 5% CO2. Fresh IL-2 and IL-7 were added every 3–4 d. After 7 d, 3–4 million PBMC CD8+ T cells were cocultured with peptide-pulsed DCs and cytokines (20–40:1 ratio). Third and fourth stimulations were done using 4–5 million CD8+ T cells and peptide-pulsed irradiated B cells (ratio of 4:1; 30 Gy) and fresh IL-2 and IL-7 (days 14 and 21). CD8+ T cell responses were then evaluated by IFNγ ELISpot assay (Mabtech) using peptide-pulsed B cells (1:1 ratio) as target cells. CD8+ T cells were purified the day before the ELISpot and were rested overnight in medium without cytokines. The ELISpot assay was performed with heat-inactivated FBS as recommended by the manufacturer. When the human material was limited, PBMCs or B cells were used in the first round of stimulation (Extended Data Fig. 9d).

LC–MS/MS analysis of pan-HLA immune peptidomes

Detailed methods for the affinity purification of MHC class I complexes and LC–MS/MS analysis have been previously described66,67.

Affinity capture of peptide–MHC for LC–DIAMS

Adherent cells were released into suspension by incubation in non-enzymatic cell dissociation medium (NECDM; PBS (pH 7.2), 1% FBS, 10 mM EDTA and 10 mM EGTA) for 1 h at 37 °C. Cells were washed in NECDM (900g, 5 min, 4 °C) and resuspended to 106 cells per ml in NECDM. For each sample, 106 cells were pelleted by centrifugation, and the pellet was gently resuspended in 1 ml of digitonin extraction buffer (0.15 mM digitonin, 75 mM sucrose, 25 mM NaCl, 2.5 mM PIPES (pH 6.8), 1 mM EDTA, 0.8 mM MgCl2 and protease inhibitor cocktail (cØmplete, Roche)). After incubation on ice for exactly 10 min, the permeabilized cells were pelleted by centrifugation (480g, 10 min, 4 °C) and resuspended in Triton X-100/alkylation buffer (0.5% Triton X-100, 75 mM sucrose, 25 mM NaCl, 2.5 mM PIPES (pH 7.4), 4 mM EDTA, 0.8 mM MgCl2 and protease inhibitor cocktail (cØmplete, Roche); when cysteines were alkylated, iodoacetamide was added to a final concentration of 10 mM just before use). After incubation for 30 min on ice, the nuclei were pelleted by centrifugation (5,000g, 10 min, 4 °C), and the clarified supernatant was transferred to new tubes (1.5-ml, low protein-binding tubes; Eppendorf). Triton X-100 was added to bring the proportion to 1.5%, together with Protein A agarose beads (10 µl packed volume) and anti-HLA-A, anti-HLA-B and anti-HLA-C monomorphic determinant (4 µg; clone W6/32, Biolegend), followed by rotation for 3 h at 4 °C. Following centrifugation (900g for 2 min at 4 °C and used in all subsequent steps), the agarose bead pellet was washed six times in octyl β-d-glucopyranoside wash buffer (1 ml; 1.75% octyl β-d-glucopyranoside, 400 mM NaCl, 40 mM Tris-HCl (pH 7.6) and 1 mM EDTA), followed by two washes in salt wash buffer (400 mM NaCl, 40 mM Tris-HCl (pH 7.6) and 1 mM EDTA). After removal of the supernatant, pelleted beads with bound immunoprecipitate were stored at –80 °C before peptide elution for MS.

Sample preparation for LC–DIAMS

Beads were washed with 200 µl of 5% acetonitrile (Fisher Chemical, HPLC grade) in water (Pierce water, LC–MS grade, Thermo Scientific) three times and transferred to a clean 0.5-ml tube (LoBind, Eppendorf), and all fluid was aspirated leaving wet beads. Fifteen microliters of 0.2% trifluoroacetic acid (Optima LC–MS Fisher Chemical) and a set of 40 retention time peptides (JPT Peptide Technologies) at 250 attomoles per peptide were added to the beads. The bead/ acid mixture was set at 65 °C for 5 min and extracted with a C18 tip (Zip Tip, Millipore Sigma). The tip was washed with 0.2% trifluoroacetic acid in water five times, followed by 0.1% formic acid (99+%, Thermo Scientific) in water (three times). Peptides were eluted into 2–3 µl of 60% methanol (Fisher Chemical, HPLC grade) in water, the volume was reduced under N2 stream, and 0.1% formic acid was added to form 1 µl for loading the trapping column with a helium-driven pressure bomb.

Chromatography for LC–DIAMS

Alkane-modified polystyrene-divinylbenzene monoliths in 20- and 50-µm ID silica capillaries were synthesized in-house for analytical and trapping columns, respectively:68 Ninety-minute segmented linear gradients from 0 to 40% acetonitrile in water (both solvents, 0.1% formic acid) were used with the segmentation varying somewhat depending on the column in use. Flow rates varied with columns but were under 10 ml min–1.

LC–DIAMS analysis

A Sciex 6600+ quadrupole-oTOF was used for all experiments. For extracting reference fragmentation patterns from synthetic peptide sets (JPT Peptide Technologies), the instrument was operated in data-dependent acquisition mode. The synthetic sets were simple, consisting of orders for 250–400 pooled peptides, and were analyzed at a nominal 150 or 300 attomoles per peptide in 0.5 or 1 µl loading. For elution mapping of the synthetic set and all sample runs, the instrument was operated in data-independent acquisition mode. The instrument collects a full-range mass spectrum followed by 11 MS/MS spectra in which the quadrupole filter is set to transmit an m/z window (the width varies over the 11) such that the union of these windows covers the m/z range of interest. In this way, all precursor molecular ions are fragmented, but each fragmentation pattern is embedded in a complex background of other coselected molecular ions. The sequence of MS and 11 MS/MS collections is repeated through the LC elution.

MS data analysis

Poisson LC–DIAMS is a targeted form of data analysis in contrast to targeted MS data acquisition and analysis. Fragmentation patterns and relative elution positions for all targets are necessary input parameters and are acquired from synthetic peptides. A formal treatment of sampling a finite event stochastic Poisson process69 generates a Kullback– Leibler cross-entropy measure that is used to identify the elution of a target's fragmentation pattern in an MS/MS window. A chromatogram of this measure is plotted against an XIC for the target's precursor m/z and displayed as a Poisson plot (Fig. 7c). Coincident XIC and Poisson peaks for a target are further qualified by their position in the chromatogram. Retention time peptides added to the data-independent acquisition runs of the synthetic set and sample generate a mapping of target elution positions from the synthetic into sample data. Peak coincidences outside the expected scatter in the elution map are not detections. Further qualification arises in inspecting the fragment XICs. These must be consistent with the precursor ion XIC elution profile and the relative amplitudes of the synthetic pattern given the fragment background and the finite event sampling or shot noise. The mass accuracy of the instrument and calibration must be satisfied. For the 6600+, mass resolution of the precursor m/z is roughly 30,000, while that of the MS/MS spectra is 25,000 with added retention time peptides validating calibration.

Prediction of peptide binding

Potential binders to NCI-H2228 HLA I (HLA-A*0201, HLA-A*0301, HLA-B*0702, HLA-B*3801, HLA-C*0702 and HLA-C*1203) were calculated using NetMHC4.0, NetMHCpan4.1 and HLAthena (with and without peptide context)66. The full set of ALK peptides that were predicted, synthesized and for which fragmentation patterns and elution positions could be experimentally established is listed in Supplementary Table 7.

CPTAC and TCGA datasets

National Cancer Institute's CPTAC LUAD44 and TCGA LUAD gene expression (http://cancergenome.nih.gov) and mutation datasets were downloaded from the GDC data portal. ALK fusions were determined using the Arriba and STAR-fusion pipelines. Only

pathogenic KRAS and EGFR mutations were considered mutant cases (CPTAC-3 LUAD (n = 110), ALK fusion (n = 7), KRAS mutant (n = 32), EGFR mutant (n = 35), TCGA LUAD (n = 516), ALK fusion (n = 4), KRAS mutant (n = 155), EGRF mutant (n = 56)). The transcripts per million normalized gene expression values as well as protein levels were plotted using the ggplot2 R package.

ALK, HLA-A, HLA-B and HLA-C mRNA expression

The expression of ALK, HLA-A, HLA-B and HLA-C mRNA in different human tissues was plotted according to the publicly available database Genotype–Tissue Expression (GTEx) Project (www.gtexportal. org/home/gene/ALK, www.gtexportal.org/home/gene/HLA-A, www. gtexportal.org/home/gene/HLA-B and https://www.gtexportal.org/ home/gene/HLA-C).

Statistics and reproducibility

All transgenic mice included in this study were verified for their genotype, and inbred animals were excluded when 2 weeks of age different. All animals were randomized by cage. Investigators were not blinded to mouse allocation after treatment administration and/or during outcome analysis. No statistical methods were used to predetermine sample sizes. Data distribution was assumed to be normal; however, this was not formally tested.

Statistical analyses were performed using GraphPad Prism software (RRID: SCR_002798). A P value of ≤0.05 was considered statistically significant. No animals or data were excluded from the analysis.

Illustrations

All graphic illustrations were created with Biorender.com.

Reporting summary

Further information on research design is available in the Nature Portfolio

Reporting Summary linked to this article.

Data availability

The MS data are deposited at https://massive.ucsd.edu/ProteoSAFe/ static/massive.jsp (Username: MSV000089110; Password: “a”) under the following dataset: MSV000089110. Data were downloaded from GTEx Project (www.gtexportal.org), TCGA (http://cancergenome.nih.gov) and CPTAC (https://cptac-data-portal. georgetown.edu/cptac/s/S056). Source data are provided with this paper. All other data are available from the authors upon reasonable request

References

1. Shaw, A. T. et al. Ceritinib versus chemotherapy in patients with *ALK*-rearranged non-small-cell lung cancer previously given chemotherapy and crizotinib (ASCEND-5): a randomised, controlled, open-label, phase 3 trial. *Lancet Oncol.* **18**, 874–886 (2017).
2. Peters, S. et al. Alectinib versus crizotinib in untreated ALK-positive non-small-cell lung cancer. *N. Engl. J. Med.* **377**, 829–838 (2017).
3. Kwak, E. L. et al. Anaplastic lymphoma kinase inhibition in non-small-cell lung cancer. *N. Engl. J. Med.* **363**, 1693–1703 (2010).
4. Shaw, A. T. et al. First-line lorlatinib or crizotinib in advanced ALK-positive lung cancer. *N. Engl. J. Med.* **383**, 2018–2029 (2020).
5. Camidge, D. R. et al. Brigatinib versus crizotinib in ALK-positive non-small-cell lung cancer. *N. Engl. J. Med.* **379**, 2027–2039 (2018).
6. Camidge, D. R. et al. Brigatinib versus crizotinib in ALK inhibitor-naive advanced ALK-positive NSCLC: final results of phase 3 ALTA-1L trial. *J. Thorac. Oncol.* **16**, 2091–2108 (2021).
7. Schneider, J. L., Lin, J. J. & Shaw, A. T. ALK-positive lung cancer: a moving target. *Nat. Cancer* **4**, 330–343 (2023).
8. Katayama, R. et al. Two novel ALK mutations mediate acquired resistance to the next-generation ALK inhibitor alectinib. *Clin. Cancer Res.* **20**, 5686–5696 (2014).
9. Gainor, J. F. et al. Molecular mechanisms of resistance to first- and second-generation ALK inhibitors in *ALK*-rearranged lung cancer. *Cancer Discov.* **6**, 1118–1133 (2016).
10. Sharma, G. G. et al. Tumor resistance against ALK targeted therapy—where it comes from and where it goes. *Cancers* **10**, 62 (2018).
11. Camidge, D. R. et al. Updated efficacy and safety data and impact of the EML4–ALK fusion variant on the efficacy of alectinib in untreated ALK-positive advanced non-small cell lung cancer in the global phase III ALEX study. *J. Thorac. Oncol.* **14**, 1233–1243 (2019).
12. Shaw, A. T. et al. *ALK* resistance mutations and efficacy of lorlatinib in advanced anaplastic lymphoma kinase-positive non-small-cell lung cancer. *J. Clin. Oncol.* **37**, 1370–1379 (2019).
13. Zhang, I., Zaorsky, N. G., Palmer, J. D., Mehra, R. & Lu, B. Targeting brain metastases in *ALK*-rearranged non-small-cell lung cancer. *Lancet Oncol.* **16**, e510–e521 (2015).
14. Johung, K. L. et al. Extended survival and prognostic factors for patients with *ALK*-rearranged non-small-cell lung cancer and brain metastasis. *J. Clin. Oncol.* **34**, 123–129 (2016).
15. Sankar, K., Nagrath, S. & Ramnath, N. Immunotherapy for *ALK*-rearranged non-small cell lung cancer: challenges inform promising approaches. *Cancers* **13**, 1476 (2021).

16. Gainor, J. F. et al. *EGFR* mutations and *ALK* rearrangements are associated with low response rates to PD-1 pathway blockade in non-small cell lung cancer: a retrospective analysis. *Clin. Cancer Res.* **22**, 4585–4593 (2016).

17. Negrao, M. V. et al. Oncogene-specific differences in tumor mutational burden, PD-L1 expression, and outcomes from immunotherapy in non-small cell lung cancer. *J. Immunother. Cancer* **9**, e002891 (2021).

18. Shi, Y. et al. Integration of comprehensive genomic profiling, tumor mutational burden, and PD-L1 expression to identify novel biomarkers of immunotherapy in non-small cell lung cancer. *Cancer Med.* **10**, 2216–2231 (2021).

19. Zeng, C. et al. Tumor-infiltrating $CD8^+$ T cells in ALK-positive lung cancer are functionally impaired despite the absence of PD-L1 on tumor cells. *Lung Cancer* **150**, 139–144 (2020).

20. Fang, Y. et al. Comprehensive analyses reveal TKI-induced remodeling of the tumor immune microenvironment in EGFR/ALK-positive non-small-cell lung cancer. *Oncoimmunology* **10**, 1951019 (2021).

21. Cheever, M. A. et al. The prioritization of cancer antigens: a national cancer institute pilot project for the acceleration of translational research. *Clin. Cancer Res.* **15**, 5323–5337 (2009).

22. Ait-Tahar, K. et al. B and CTL responses to the ALK protein in patients with ALK-positive ALCL. *Int. J. Cancer* **118**, 688–695 (2006).

23. Ait-Tahar, K. et al. Correlation of the autoantibody response to the ALK oncoantigen in pediatric anaplastic lymphoma kinase-positive anaplastic large cell lymphoma with tumor dissemination and relapse risk. *Blood* **115**, 3314–3319 (2010).

24. Singh, V. K. et al. NPM–ALK-reactive T-cell responses in children and adolescents with NPM–ALK positive anaplastic large cell lymphoma. *Oncoimmunology* **8**, e1625688 (2019).

25. Knorr, F. et al. Epitope mapping of anti-ALK antibodies in children with anaplastic large cell lymphoma. *Clin. Immunol.* **195**, 77–81 (2018).

26. Passoni, L. et al. In vivo T-cell immune response against anaplastic lymphoma kinase in patients with anaplastic large cell lymphomas. *Haematologica* **91**, 48–55 (2006).

27. Awad, M. M. et al. Epitope mapping of spontaneous autoantibodies to anaplastic lymphoma kinase (ALK) in non-small cell lung cancer. *Oncotarget* **8**, 92265–92274 (2017).

28. Chiarle, R. et al. The anaplastic lymphoma kinase is an effective oncoantigen for lymphoma vaccination. *Nat. Med.* **14**, 676–680 (2008).

29. Voena, C. et al. Efficacy of a cancer vaccine against *ALK*-rearranged lung tumors. *Cancer Immunol. Res.* **3**, 1333–1343 (2015).

30. Passoni, L. et al. ALK as a novel lymphoma-associated tumor antigen: identification of 2 HLA-A2.1-restricted $CD8^+$ T-cell epitopes. *Blood* **99**, 2100–2106 (2002).

31. Maddalo, D. et al. In vivo engineering of oncogenic chromosomal rearrangements with the CRISPR/Cas9 system. *Nature* **516**, 423–427 (2014).

32. Blasco, R. B. et al. Simple and rapid in vivo generation of chromosomal rearrangements using CRISPR/Cas9 technology. *Cell Rep.* **9**, 1219–1227 (2014).

33. Gainor, J. F. et al. *EGFR* mutations and *ALK* rearrangements are associated with low response rates to PD-1 pathway blockade in non-small cell lung cancer (NSCLC): a retrospective analysis. *Clin. Cancer Res.* **22**, 4585–4593 (2016).

34. Chiarle, R., Voena, C., Ambrogio, C., Piva, R. & Inghirami, G. The anaplastic lymphoma kinase in the pathogenesis of cancer. *Nat. Rev. Cancer* **8**, 11–23 (2008).

35. Dantoing, E., Piton, N., Salaun, M., Thiberville, L. & Guisier, F. Anti-PD1/PD-L1 immunotherapy for non-small cell lung cancer with actionable oncogenic driver mutations. *Int. J. Mol. Sci*. **22**, 6288 (2021).

36. Wang, L. & Lui, V. W. Y. Emerging roles of ALK in immunity and insights for immunotherapy. *Cancers* **12**, 426 (2020).

37. Powis, S. J. et al. Restoration of antigen presentation to the mutant cell line RMA-S by an MHC-linked transporter. *Nature* **354**, 528–531 (1991).

38. Palmer, R. H., Vernersson, E., Grabbe, C. & Hallberg, B. Anaplastic lymphoma kinase: signalling in development and disease. *Biochem. J.* **420**, 345–361 (2009).

39. Horton, B. L. et al. Lack of $CD8^+$ T cell effector differentiation during priming mediates checkpoint blockade resistance in non-small cell lung cancer. *Sci. Immunol.* **6**, eabi8800 (2021).

40. Le, D. T. et al. Evaluation of ipilimumab in combination with allogeneic pancreatic tumor cells transfected with a GM–CSF gene in previously treated pancreatic cancer. *J. Immunother.* **36**, 382–389 (2013).

41. Gubin, M. M. et al. Checkpoint blockade cancer immunotherapy targets tumour-specific mutant antigens. *Nature* **515**, 577–581 (2014).

42. Keskin, D. B. et al. Neoantigen vaccine generates intratumoral T cell responses in phase Ib glioblastoma trial. *Nature* **565**, 234–239 (2019).

43. Mahadevan, N. R. et al. Intrinsic Immunogenicity of small cell lung carcinoma revealed by its cellular plasticity. *Cancer Discov.* **11**, 1952–1969 (2021).

44. Gillette, M. A. et al. Proteogenomic characterization reveals therapeutic vulnerabilities in lung adenocarcinoma. *Cell* **182**, 200–225 (2020).

45. Keskin, D. B. et al. Direct identification of an HPV-16 tumor antigen from cervical cancer biopsy specimens. *Front. Immunol.* **2**, 75 (2011).

46. Reinherz, E. L., Keskin, D. B. & Reinhold, B. Forward vaccinology: CTL targeting based upon physical detection of HLA-bound peptides. *Front. Immunol.* **5**, 418 (2014).

47. Blasco, R. B., Patrucco, E., Mota, I., Tai, W. T. & Chiarle, R. Comment on "ALK is a therapeutic target for lethal sepsis". *Sci. Transl. Med*. **10**, eaar4321 (2018).

48. Martinez, P., Peters, S., Stammers, T. & Soria, J. C. Immunotherapy for the first-line treatment of patients with metastatic non-small cell lung cancer. *Clin. Cancer Res.* **25**, 2691–2698 (2019).

49. Petrazzuolo, A. et al. Pharmacological inhibitors of anaplastic lymphoma kinase (ALK) induce immunogenic cell death through on-target effects. *Cell Death Dis.* **12**, 713 (2021).

50. Hegde, S. et al. Dendritic cell paucity leads to dysfunctional immune surveillance in pancreatic cancer. *Cancer Cell* **37**, 289–307 (2020).

51. Zagorulya, M. et al. Tissue-specific abundance of interferon-γ drives regulatory T cells to restrain DC1-mediated priming of cytotoxic T cells against lung cancer. *Immunity* **56**, 386–405 (2023).

52. Herbst, R. S. et al. Predictive correlates of response to the anti-PD-L1 antibody MPDL3280A in cancer patients. *Nature* **515**, 563–567 (2014).

53. Sanmamed, M. F. et al. A Burned-out $CD8^+$ T-cell subset expands in the tumor microenvironment and curbs cancer immunotherapy. *Cancer Discov.* **11**, 1700–1715 (2021).

54. Baumeister, S. H., Freeman, G. J., Dranoff, G. & Sharpe, A. H. Coinhibitory pathways in immunotherapy for cancer. *Annu. Rev. Immunol.* **34**, 539–573 (2016).

55. Pedicord, V. A., Montalvo, W., Leiner, I. M. & Allison, J. P. Single dose of anti-CTLA-4 enhances $CD8^+$ T-cell memory formation, function, and maintenance. *Proc. Natl Acad. Sci. USA* **108**, 266–271 (2011).

56. Sharma, N., Vacher, J. & Allison, J. P. TLR1/2 ligand enhances antitumor efficacy of CTLA-4 blockade by increasing intratumoral T_{reg} depletion. *Proc. Natl Acad. Sci. USA* **116**, 10453–10462 (2019).

57. McGranahan, N. et al. Allele-specific HLA loss and immune escape in lung cancer evolution. *Cell* **171**, 1259–1271 (2017).

58. Tran, E. et al. T-cell transfer therapy targeting mutant *KRAS* in cancer. *N. Engl. J. Med.* **375**, 2255–2262 (2016).

59. Le Naour, J., Zitvogel, L., Galluzzi, L., Vacchelli, E. & Kroemer, G. Trial watch: STING agonists in cancer therapy. *Oncoimmunology* **9**, 1777624 (2020).

60. Stronen, E. et al. Targeting of cancer neoantigens with donor-derived T cell receptor repertoires. *Science* **352**, 1337–1341 (2016).

61. Reynisson, B., Alvarez, B., Paul, S., Peters, B. & Nielsen, M. NetMHCpan-4.1 and NetMHCIIpan-4.0: improved predictions of MHC antigen presentation by concurrent motif deconvolution and integration of MS MHC eluted ligand data. *Nucleic Acids Res.* **48**, W449–W454 (2020).

62. Andreatta, M. & Nielsen, M. Gapped sequence alignment using artificial neural networks: application to the MHC class I system. *Bioinformatics* **32**, 511–517 (2016).

63. Liu, H. et al. Structure-based programming of lymph-node targeting in molecular vaccines. *Nature* **507**, 519–522 (2014).

64. Schultze, J. L. et al. Follicular lymphomas can be induced to present alloantigen efficiently: a conceptual model to improve their tumor immunogenicity. *Proc. Natl Acad. Sci. USA* **92**, 8200–8204 (1995).

65. Liebig, T. M., Fiedler, A., Zoghi, S., Shimabukuro-Vornhagen, A. & von Bergwelt-Baildon, M. S. Generation of human CD40-activated B cells. *J. Vis. Exp.* https://doi.org/10.3791/1373 (2009).

66. Sarkizova, S. et al. A large peptidome dataset improves HLA class I epitope prediction across most of the human population. *Nat. Biotechnol.* **38**, 199–209 (2020).

67. Klaeger, S. et al. Optimized liquid and gas phase fractionation increases HLA–peptidome coverage for primary cell and tissue samples. *Mol. Cell. Proteomics* **20**, 100133 (2021).

68. Gregus, M., Kostas, J. C., Ray, S., Abbatiello, S. E. & Ivanov, A. R. Improved sensitivity of ultralow flow LC–MS-based proteomic profiling of limited samples using monolithic capillary columns and FAIMS technology. *Anal. Chem.* **92**, 14702–14712 (2020).

69. Reinhold, B., Keskin, D. B. & Reinherz, E. L. Molecular detection of targeted major histocompatibility complex I-bound peptides using a probabilistic measure

and nanospray MS3 on a hybrid quadrupole-linear ion trap. *Anal. Chem.* **82**, 9090–9099 (2010).

Acknowledgements

We thank N. Chamberlin for editing of the manuscript and M. S. Scalzo, R. Dall'Olio, P. Le, L. Li, S. Peola and B. Castella for technical assistance. I.M. was supported by the European Union Horizon 2020 Marie Skłodowska–Curie Innovative Training Network Grant (675712) for the European Research Initiative for ALK-Related Malignancies (ERIA). R.B.B. was supported by a fellowship from the Ramon Areces Foundation. The work was supported by TRP Pilot grants from the Boston Children's Hospital (to R.C.), by the Bridge Project, a partnership between the Koch Institute for Integrative Cancer Research at MIT and the Dana-Farber/Harvard Cancer Center (to D.J.I. and R.C.), the Koch Institute Dana–Farber/Harvard Cancer Center Extended Bridge Project (to D.J.I., M.M.A. and R.C.), the DFCI Lung Cancer Development Award and ALK Positive/LUNGevity Lung Cancer Research Awards (to M.M.A. and R.C.), the 1 P50 CA265826-01A1 Dana–Farber/Harvard Cancer Center SPORE in Lung Cancer (to R.C, D.A.B. and M.M.A.), the Ellison Foundation Boston grant (to R.C.), the Grant for Oncology Innovation from Merck Healthcare KGaA (to R.C.), a Pfizer research grant 53232955 (to R.C.), the V Foundation (to D.J.I.) and the NIH (EB022433; to D.J.I.). D.B.K. and C.J.W. are supported in part by NIH/NCI U24CA224331. D.B.K. is supported by 1R01HL157174- 01A1. Z.M.S. and Z.S. were supported by the Department of Defense through the Lung Cancer Research Program (award number W81XWH-18-1-0751) and the Breast Cancer Research Foundation (BCRF-21-159). E.B. was supported by the American–Italian Cancer Foundation fellowship. T.-C.C. is supported by a OFD/BTREC/CTREC Career Development Fellowship. C.A. is supported by the Giovanni Armenise–Harvard Foundation, the International Lung Cancer Foundation, the European Research Council under the European Union's Horizon 2020 research and innovation programme (grant agreement number 101001288), AIRC under IG 2021 ID 25737 project and the Zanon di Valgiurata family through Justus s.s. Author contributions I.M., R.B.B. and R.C. conceptualized the study. I.M., E.P., C.M., N.R.M., T.C.T., G.L., E.K.A., M.C., T.P., M.M., C.A., D.L.L., D.B.K., J.S.D.-C., B.R., K.D.M., C.V. and R.B.B. performed in vitro experiments. S.K., H.K. and S.A.C. performed MS experiments. J.S.D.-C. and B.R. performed LC–DIAMS experiments. I.M., E.B., T.-C.C., E.P., C.M., T.P., M.M. and R.B.B. performed mouse experiments. Z.M.S. and Z.S. analyzed CPTAC and TCGA datasets. I.M., D.B.K., J.S.D.-C., B.R., K.D.M., C.V., R.B.B. and R.C. analyzed data. C.J.W., D.A.B., D.J.I., M.M.A. and E.L.R. supervised experiments and analyzed data. M.M.A. provided human samples. I.M., N.R.M., M.M.A., D.A.B., E.L.R., R.B.B. and R.C. wrote and edited the manuscript. Competing interests R.C. and R.B.B. have filed IP related to human ALK vaccine sequences. R.C. and D.J.I. hold stock options in Elicio Therapeutics. D.J.I. is a consultant to Elicio Therapeutics. R.B.B. is a current employee of Moderna Therapeutics. C.J.W. receives research funding from Pharmacyclics and holds equity in BioNTech, Inc. D.B.K. is a scientific advisor for Immunitrack

and Breakbio. D.B.K. owns equity in Afimed N.V., Agenus, Armata Pharmaceuticals, Breakbio, BioMarin Pharmaceutical, Celldex Therapeutics, Editas Medicine, Gilead Sciences, Immunitybio, ImmunoGen, IMV, Lexicon Pharmaceuticals and Neoleukin Therapeutics. BeiGene, a Chinese biotech company, supported unrelated severe acute respiratory syndrome coronavirus 2 research at Translational Immunogenomics Lab (TIGL) at DFCI. Additional information Extended data is available for this paper at https://doi.org/10.1038/s43018-023-00591-2. Supplementary information The online version contains supplementary material available at https://doi.org/10.1038/s43018-023-00591-2. Correspondence and requests for materials should be addressed to Rafael B. Blasco or Roberto Chiarle. Peer review information Nature Cancer thanks Shibin Zhou and the other, anonymous, reviewer(s) for their contribution to the peer review of this work. Reprints and permissions information is available at www.nature.com/reprints. Publisher's note Springer Nature remains neutral with regard to jurisdictional claims in published maps and institutional afiliations. Mouse studies were approved by the IACUC committee at Boston Children's Hospital. Further information on research design is available in the Nature Research Reporting Summary linked to this article The remaining authors declare no competing interests.

Fig. 1 | ICIs do not increase the efficacy of ALK TKIs in ALK+ lung cancer mouse models. a, Representative hematoxylin and eosin (H&E) staining of hEML4–ALK-rearranged lung tumor tissue in hEML4–ALK-transgenic mice (n = 5 mice; left) and Ad-EA mice (n = 5 mice; right); scale bars, 100 μm. b, Coronal T2-weighted MRI lung sections of a representative Ad-EA mouse receiving 15 d of lorlatinib treatment combined with anti-PD-1. Yellow arrows indicate tumor lesions. c,d, Schematic representation of the treatment protocol in hEML4–ALKtransgenic (c) and Ad-EA (d) mice; Pre, before treatment; BID, twice a day. e–g, Quantification of volume changes compared to baseline tumor volume in hEML4–ALK-transgenic mice treated as in c at the end of treatment (T0; e), 4 weeks after treatment suspension (T4; f) and 8 weeks after treatment suspension (T8; g). Data are shown as change from baseline (percent ± s.e.m.; n = 3 mice per group). h–j, Quantification of volume changes compared to baseline tumor volume in Ad-EA mice treated as in d at T0 (h), T4 (i) and T8 (j). Data are shown as change from baseline (percent ± s.e.m.; n = 4 mice per group). Each dot represents an individual mouse. All P values displayed were calculated using an ordinary one-way analysis of variance

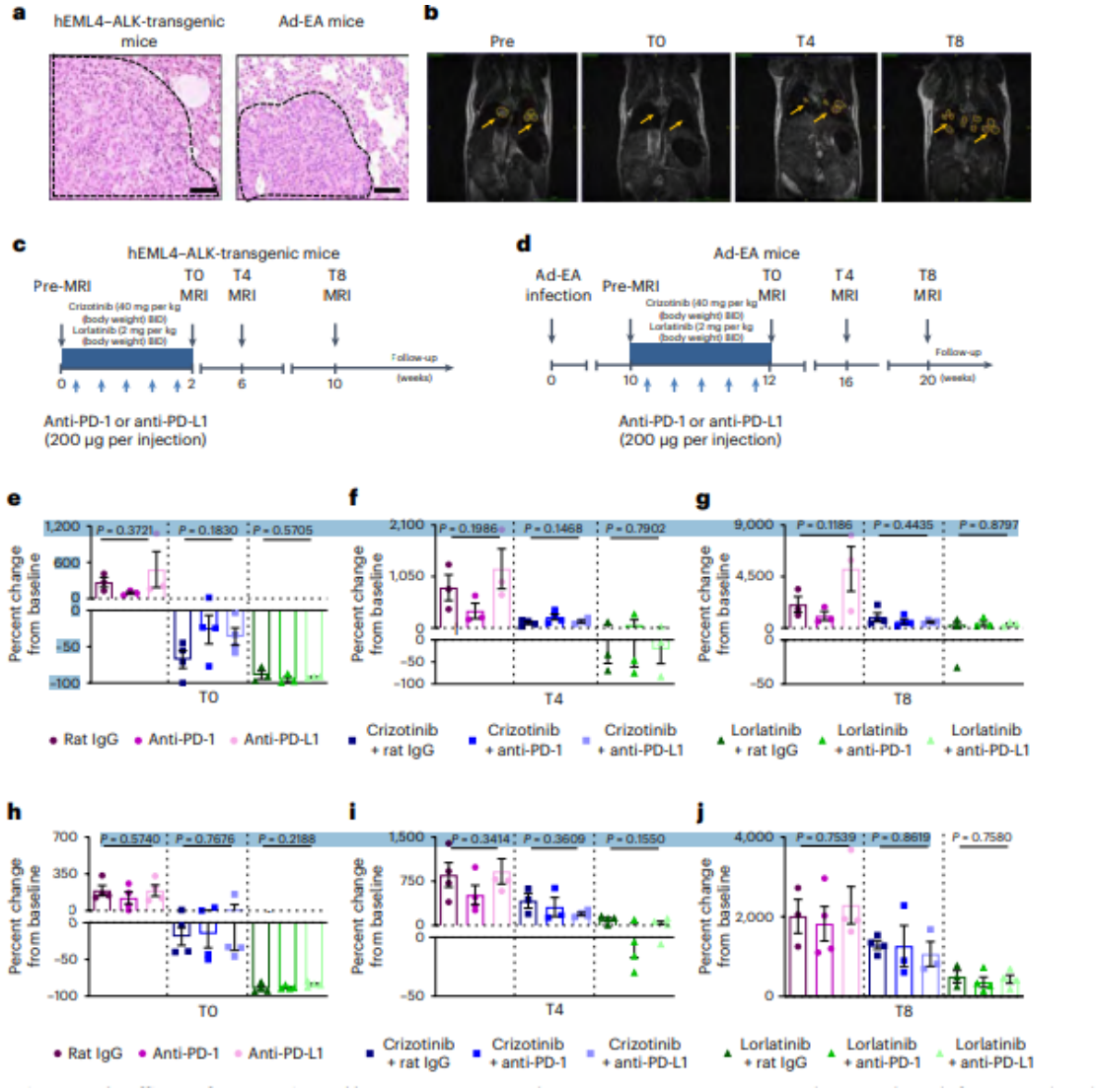

Fig. 2 | Identification of ALK immunogenic peptides in mouse models. a, IFNγ ELISpot assay of splenocytes isolated from mice vaccinated with an ALK DNA vaccine as schematically represented in Extended Data Fig. 1g. Data are from three technical replicates. A cutoff value of 100 IFNγ spot-forming units (SFU) was applied to provide a threshold of responsiveness. One of two independent biological experiments is shown. b, IFNγ ELISpot analysis of splenocytes isolated from naive mice and mice vaccinated with ALK short peptide 7 (PGPGRVAKI vax) with cyclic dinucleotide (CDN) adjuvant. Data are shown as average number of SFU ± s.e.m. Each dot represents one mouse (naive: n = 5 mice; vaccinated: n = 6 mice). c, Representative PGPGRVAKI-specific dextramer staining of splenocytes from naive mice and mice vaccinated with ALK short peptide 7 (PGPGRVAKI). Cells were gated from viable CD8+ T cells. d, Quantification by dextramer staining of PGPGRVAKI-specific CD8+ T cells isolated from splenocytes of naive mice and PGPGRVAKI-vaccinated mice displayed as

percent ± s.e.m. Each dot represents an individual mouse (naive: n = 10 mice; vaccinated: n = 5 mice). Data were analyzed by unpaired two-tailed Student's t-test. e, Quantification by dextramer staining of PGPGRVAKI-specific CD8+ T cells in splenocytes or lung TILs from 12-week-old hEML4–ALK-transgenic mice displayed as percent ± s.e.m. Each dot represents one mouse (n = 6 mice per group)

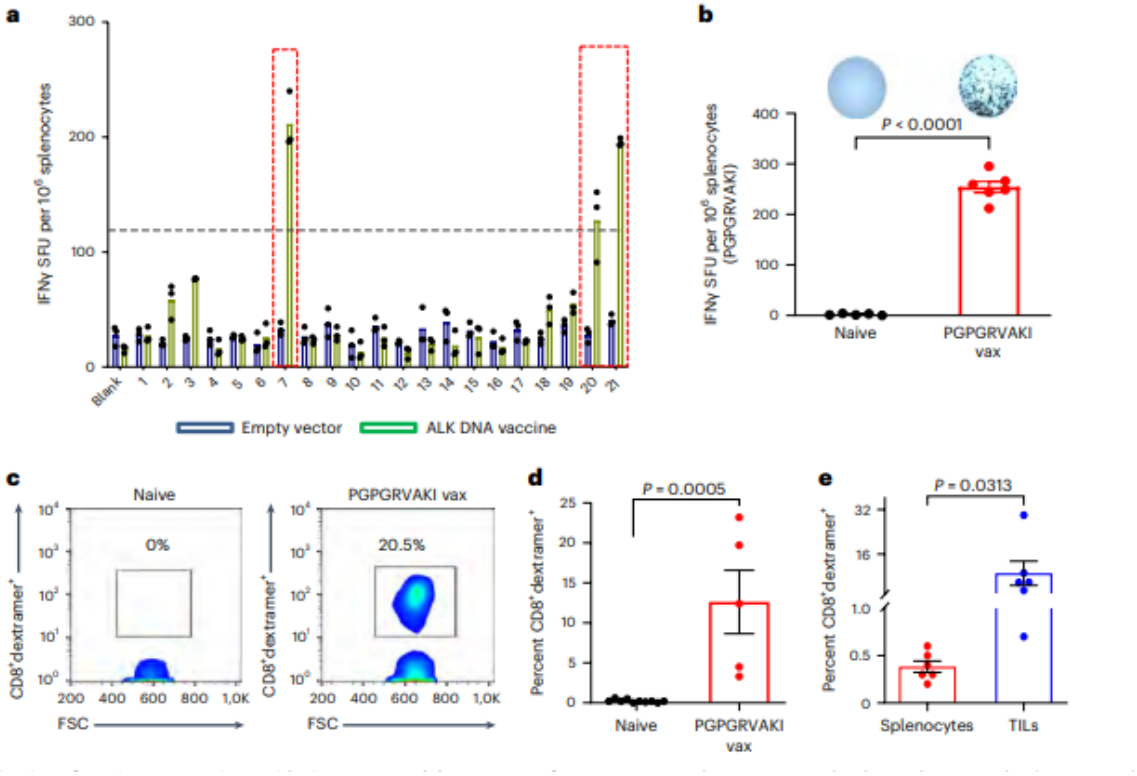

Fig. 3 | Tumor localization dictates the strength of the anti-ALK spontaneous immune response and determines the response to ICIs. a, Eml4–AlkPGPGRVAKI-1 cells were injected subcutaneously into the flanks of syngeneic BALB/c mice, and spontaneous tumor growth was measured. Two independent experiments are shown (n = 9 mice). b, Eml4–AlkPGPGRVAKI-1 cells were injected as in a, and mice were treated as indicated with anti-PD-1. Tumor growth was measured. Two independent experiments are shown (n = 10 mice). c,d, Eml4–AlkPGPGRVAKI-1 cells were injected as in a, and mice were treated as indicated (n = 11 mice). Tumor-free mice were subcutaneously rechallenged at day 50 after initial tumor injection with either mEml4–Alk (n = 5 mice) or Eml4–AlkPGPGRVAKI-1 cells (n = 5 mice), and tumor volume was monitored. e, Kaplan–Meier curves showing overall survival of mice described in a–d. Data were analyzed by log-rank test. Rechallenged mice are not shown. f, Kaplan–Meier curves showing overall survival of mice subjected to tumor rechallenge through intravenous injection with either mEml4–Alk or Eml4–AlkPGPGRVAKI-1 cells at day 100 after initial challenge. Data were analyzed by log-rank test. g, Representative H&E staining of lung

adenocarcinomas from BALB/c mice injected intravenously with Eml4–AlkPGPGRVAKI-1 cells and treated as indicated (n = 4 mice per group). Black arrows indicate lung tumors; scale bars, 1.5 mm. h, Kaplan–Meier curves showing overall survival of mice described in g. Data were analyzed by log-rank test; untreated, n = 4 mice; anti-PD-1, n = 7 mice; anti-CTLA-4, n = 7 mice; combination treatment (combo), n = 7 mice). i, IFNγ ELISpot analysis of isolated splenocytes 15 d after subcutaneous (flank) and intravenous (lung) injection of mice treated as in e and h. Data are shown as average number of SFU ± s.e.m. Each dot represents one mouse (n = 4 mice per group). Data were analyzed by unpaired two-tailed Student's t-test. j, Dextramer staining of PGPGRVAKI-specific CD8+ T cells isolated from splenocytes 15 d after subcutaneous (flank; n = 6 mice per group) and intravenous (lung; n = 4 mice per group) injection of mice treated as in e and h. Data are displayed as percent ± s.e.m. Each dot represents one mouse. Data were analyzed by unpaired two-tailed Student's t-test

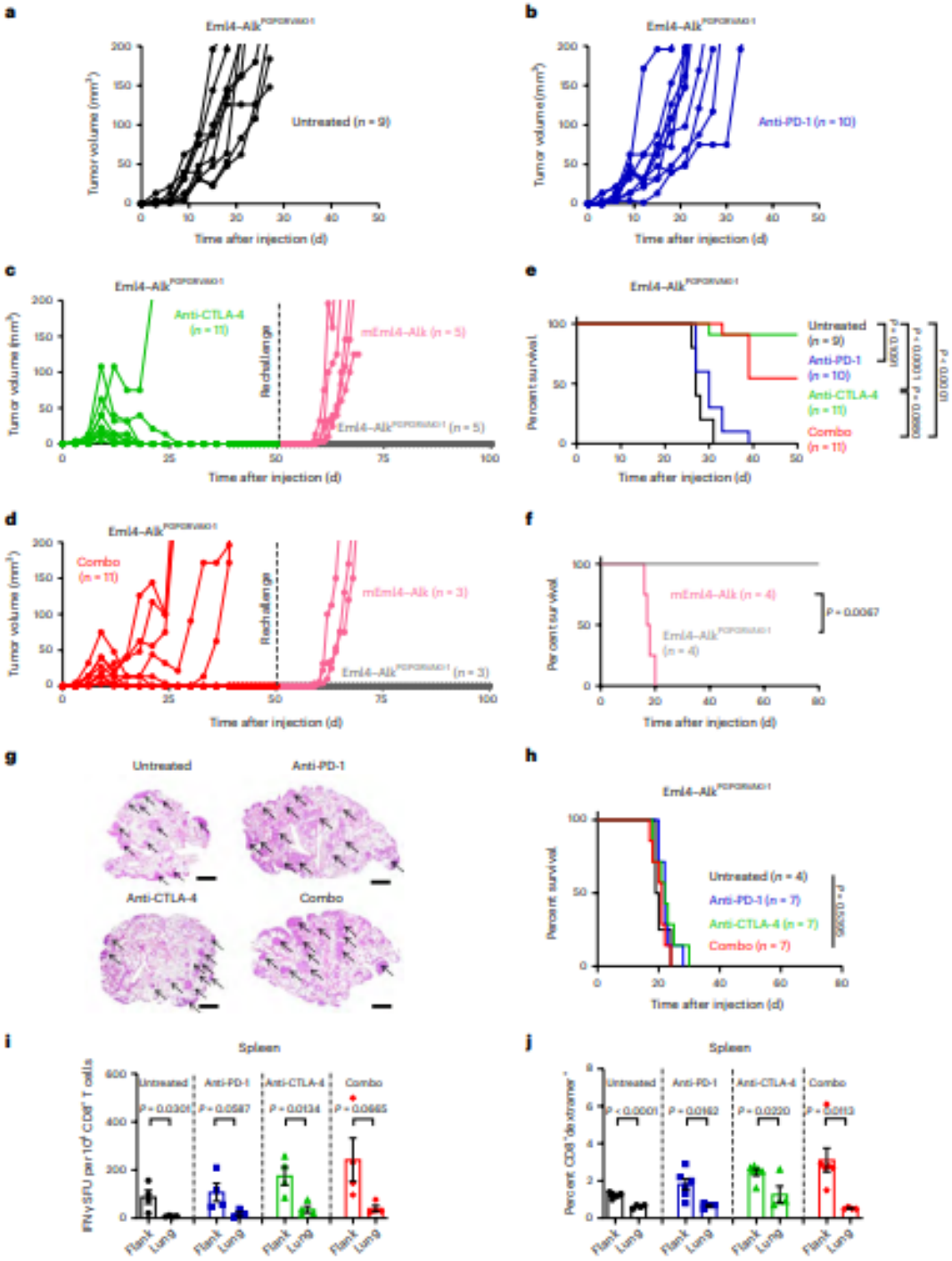
a
Eml4–Alk
Untreated (n = 9)
Tumor volume (mm³)
Time after injection (d)
b
Eml4–Alk
Anti-PD-1 (n = 10)
Tumor volume (mm³)
Time after injection (d)
c
Eml4–Alk
Anti-CTLA-4 (n = 11)
Rechallenge
mEml4–Alk (n = 5)
Eml4–Alk (n = 5)
Tumor volume (mm³)
Time after injection (d)
e
Eml4–Alk
Untreated (n = 9)
Anti-PD-1 (n = 10)
Anti-CTLA-4 (n = 11)
Combo (n = 11)
P = 0.0001
P = 0.0001
P = 0.0001
P = 0.0003
P = 0.0990
Percent survival
Time after injection (d)
d
Eml4–Alk
Combo (n = 11)
Rechallenge
mEml4–Alk (n = 3)
Eml4–Alk (n = 3)
Tumor volume (mm³)
Time after injection (d)
f
mEml4–Alk (n = 4)
Eml4–Alk (n = 4)
P = 0.0067
Percent survival
Time after injection (d)
g
Untreated
Anti-PD-1
Anti-CTLA-4
Combo
h
Eml4–Alk
Untreated (n = 4)
Anti-PD-1 (n = 7)
Anti-CTLA-4 (n = 7)
Combo (n = 7)
P = 0.0099
Percent survival
Time after injection (d)
i
Spleen
Untreated
Anti-PD-1
Anti-CTLA-4
Combo
P = 0.0301
P = 0.0587
P = 0.0134
P = 0.0665
IFNγ SFU per 10⁶ CD8⁺ T cells
Flank
Lung
j
Spleen
Untreated
Anti-PD-1
Anti-CTLA-4
Combo
P < 0.0001
P = 0.0162
P = 0.0220
P = 0.0413
Percent CD8⁺dextramer⁺
Flank
Lung

Fig. 4 | Enhancement of anti-ALK immune responses by vaccination leads to rejection of ALK+ lung tumors in combination with an ALK TKI. a, IFNγ ELISpot analysis of isolated splenocytes from BALB/c mice intravenously injected with Eml4–AlkPGPGRVAKI-1 cells (n = 21 mice) compared to tumor-free mice vaccinated with the ALK vaccine (n = 6 mice). Naive mice (n = 5) were used as negative controls. Data are shown as average number of SFU ± s.e.m. Each dot represents one mouse. Data were analyzed by unpaired two-tailed Student's t-test. b, Dextramer staining of PGPGRVAKI-specific CD8+ T cells isolated from lung TILs of untreated lung tumor-bearing mice (n = 8) and lung tumor-bearing mice vaccinated with the PGPGRVAKI peptide with CDN adjuvant (n = 6; data are shown as percent ± s.e.m.). Data were analyzed by unpaired two-tailed Student's t-test. c, PD-1 staining displayed as percent ± s.e.m. within the CD8+ ALK dextramer+ populations isolated from lung TILs of untreated (n = 8) and ALK vaccinated (n = 6) mice. Data were analyzed by unpaired two-tailed Student's t-test. d, Schematic representation of the treatment protocol in therapeutic experiments to combine the ALK vaccine (ALK vax; PGPGRVAKI peptide with CDN adjuvant) with ALK TKI and ICIs; DIE, once a day; i.v., intravenous. e, Kaplan– Meier curves showing the overall survival of mice treated as indicated in d. Data are combined from two independent experiments and were analyzed by log-rank test; NS, not significant. f, ALK dextramer staining of PGPGRVAKI-specific CD8+ T cells isolated from the peripheral blood of surviving mice (for more than 250 d) from the experiment shown in e and rechallenged intravenously with Eml4–AlkPGPGRVAKI-1 cells. Each dot represents one mouse and data are displayed as percent ± s.e.m. The number of mice per group is shown in g. g, Kaplan–Meier curves showing overall survival of mice rechallenged intravenously with Eml4– AlkPGPGRVAKI-1 cells as in f. Data were analyzed by log-rank test.

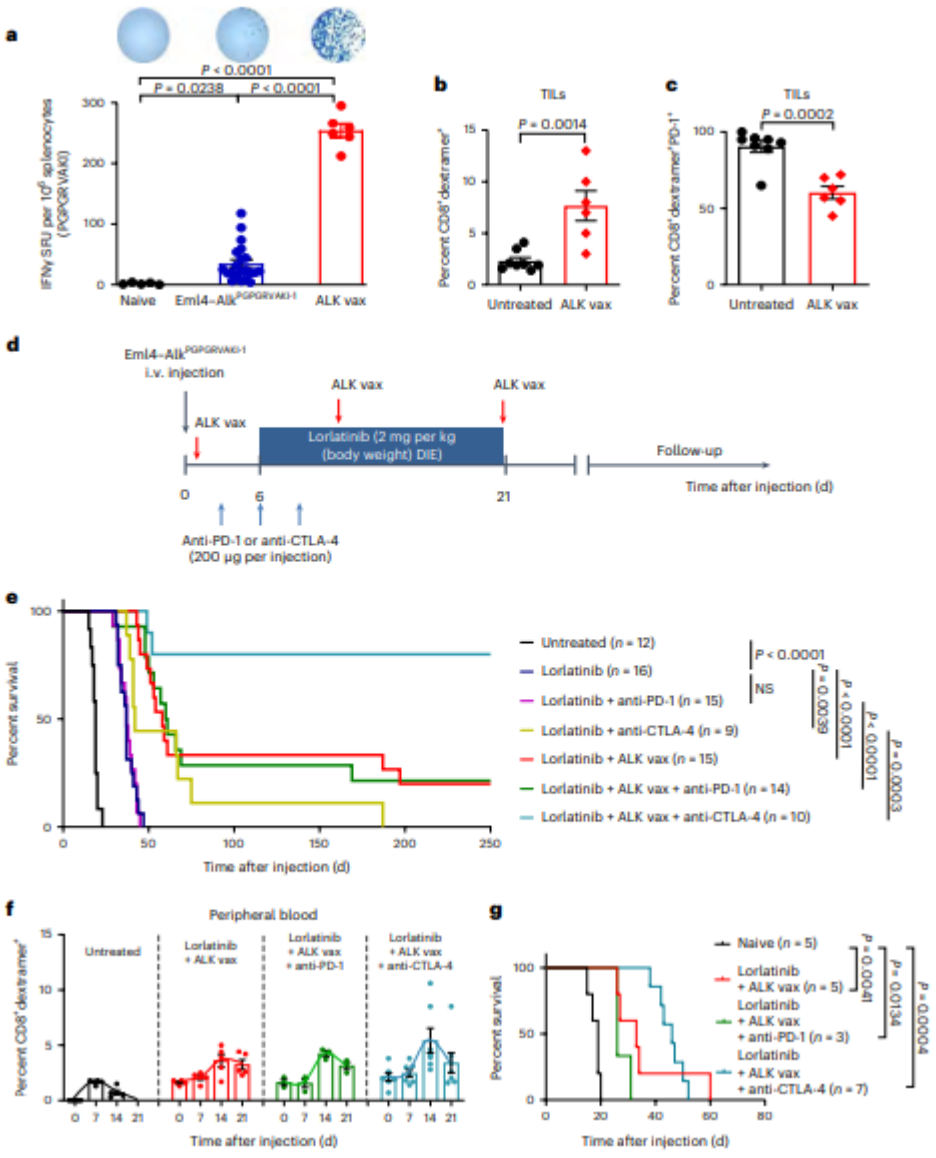

Fig. 5 | ALK vaccine prevents metastatic spread to the CNS in combination with an ALK TKI. a, Schematic representation of the metastatic assay to the CNS by intravenous injection of Eml4–AlkPGPGRVAKI-1 cells. b, Representative H&E staining of the meninges and brain tissue from BALB/c mice used in the brain metastasis assay and treated as indicated; ALK vax, PGPGRVAKI peptide with CDN adjuvant. Lorlatinib and ICI were given as in Fig. 4d; scale bars, 50 µm. The numbers of mice per treatment group are shown in c. c, Incidence of CNS metastases in mice treated with the indicated combination therapies. The numbers of mice per treatment group are shown above the bars in the graph.

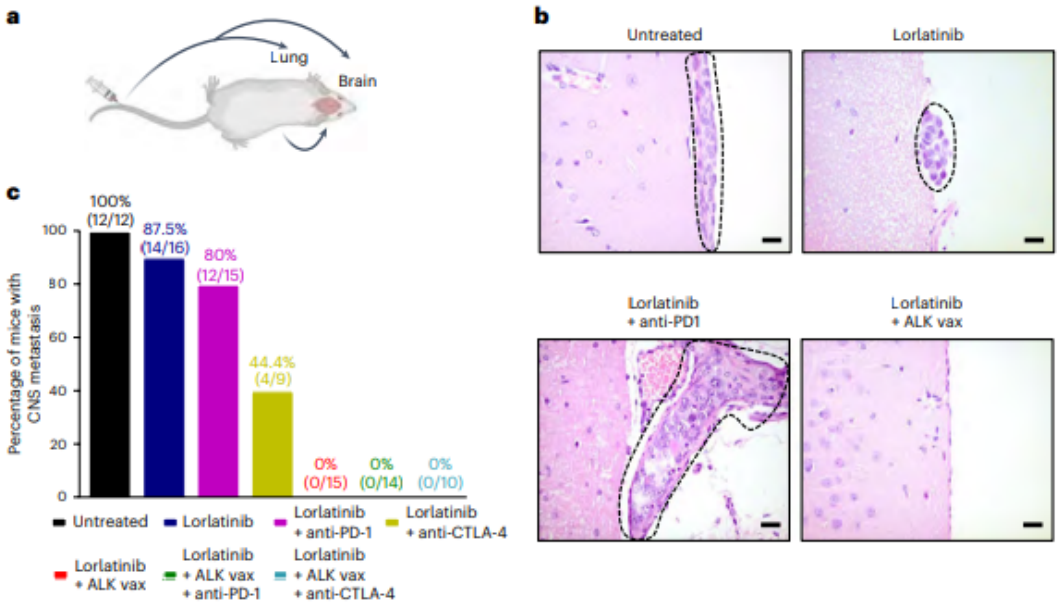

Fig. 6 | Tumor escape in vaccinated mice is due to reversible MHC class I downregulation. a, Representative H&E staining of lung adenocarcinomas from syngeneic BALB/c mice treated as described in Fig. 4d. Black arrows indicate lung tumors (n = 4 mice per group); scale bars, 1.5 mm. b, H-2Dd staining by flow cytometry of cell lines isolated from lung tumors that escaped the indicated treatment. Data are shown as mean fluorescence intensity (MFI) ± s.e.m. from mice described in Fig. 4d. Each dot represents one cell line isolated from a different tumor (untreated, n = 20; lorlatinib, n = 10; lorlatinib + anti-PD-1, n = 10; lorlatinib + anti-CTLA-4, n = 7; lorlatinib + ALK vaccine, n = 30; lorlatinib + ALK vaccine + anti-PD-1, n = 17 biologically independent ex vivo cell lines). Data were analyzed by unpaired two-tailed Student's t-test. c, H-2Dd staining displayed as MFI of MHC class Ilow cell lines isolated from lung tumors that escaped the indicated treatment and were treated for 24 h with IFNγ. Each dot represents a technical replicate, and paired columns (±IFNγ) represent individual cell lines (parental cell line and ex vivo cell lines isolated from mice treated with lorlatinib + ALK vaccine (n = 4 ex vivo cell lines) and treated with lorlatinib + ALK vaccine + anti-PD-1 (n = 3 ex vivo cell lines)). d–g, Growth curves of tumors generated by two independent MHC class Ihigh (d and e) and MHC class Ilow (f and g) cell lines that were injected subcutaneously into naive BALB/c mice and treated as indicated. Each line represents one mouse. h, H-2Dd staining of eight independent MHC class Ilow cell lines isolated from lung tumors that escaped the indicated treatment and were treated with a STING agonist (ADU-S100).

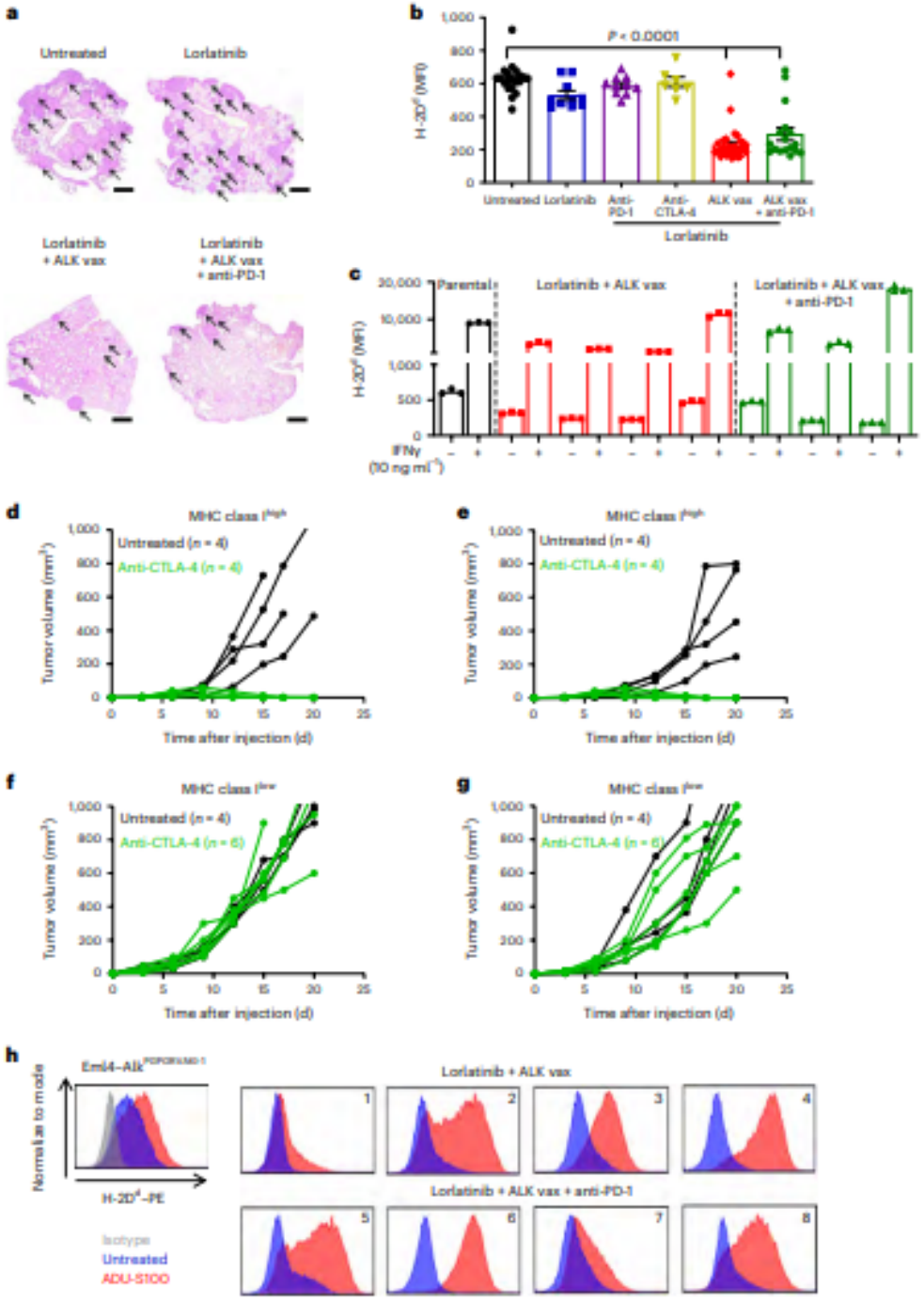
a
Untreated
Lorlatinib
Lorlatinib + ALK vax
Lorlatinib + ALK vax + anti-PD-1
b
P < 0.0001
H-2D^d (MFI)
Untreated
Lorlatinib
Anti-PD-1
Anti-CTLA-4
ALK vax
ALK vax + anti-PD-1
Lorlatinib
c
Parental
Lorlatinib + ALK vax
Lorlatinib + ALK vax + anti-PD-1
H-2D^d (MFI)
IFNγ (10 ng ml^−1)
d
MHC class I^high
Untreated (n = 4)
Anti-CTLA-4 (n = 4)
Tumor volume (mm^3)
Time after injection (d)
e
MHC class I^high
Untreated (n = 4)
Anti-CTLA-4 (n = 4)
Tumor volume (mm^3)
Time after injection (d)
f
MHC class I^low
Untreated (n = 4)
Anti-CTLA-4 (n = 6)
Tumor volume (mm^3)
Time after injection (d)
g
MHC class I^low
Untreated (n = 4)
Anti-CTLA-4 (n = 6)
Tumor volume (mm^3)
Time after injection (d)
h
Eml4–Alk^POPDRXLMD-1
Normalized to mode
H-2D^d–PE
Isotype
Untreated
ADU-S100
Lorlatinib + ALK vax
Lorlatinib + ALK vax + anti-PD-1

Fig. 7 | Identification of immunogenic ALK peptides in individuals with ALK+ NSCLC. a, H&E stainings and immunohistochemistry for ALK and MHC class I expression from representative tumors from individuals with ALK+ NSCLC (n = 10 samples); scale bars, 100 μm. b, Expression of human MHC class I and ALK in 10 treatment-naive tumors from individuals with ALK+ NSCLC as determined by immunohistochemistry and H score. An H score of ≥200 indicates high levels of protein expression, an H score of ≥100 and <200 indicates intermediate levels of protein expression, and an H score of <100 indicates low levels of protein expression. The ALK fusion variants, including EML4–ALK V1, V3, V5' and V7, are indicated for each case. c, Poisson LC–DIAMS plots from pan-HLA immunoprecipitations of the ALK+cell line NCI-H2228 (top) and a lung tumor biopsy from an individual with ALK rearranged NSCLC (middle and bottom). Poisson plots combine an extracted ion chromatogram (XIC) for peptide precursor m/z (black trace) with an inverted, scaled Poisson chromatogram (blue trace). Peptide detection at an elution point is associated with coincident precursor and Poisson peaks, here marked by blue arrows. d, Quantification of IFNγ ELISpot assays from splenocytes isolated from HLA-B*07:02-transgenic mice vaccinated with peptides IVRshort (n = 6 mice) or IVRlong (n = 6 mice; top) or RPRshort 9 (n = 6 mice) or RPRlong (n = 6 mice; bottom) with CDN adjuvant. Each bar represents SFU obtained from splenocytes isolated from an individual mouse and stimulated with either the corresponding peptide (IVRCIGVSL or RPRSQPSSL) or the peptide solvent (water). Two independent experiments were performed. Data are represented as three technical replicates from one experiment. e, Representative IFNγ ELISpot assay of CD8+ T cells isolated from participant 6 (Supplementary Table 10) and expanded in the presence of either IVRCIGVSL or RPRSQPSSL, with the protocol represented in Extended Data Fig. 9d. CD8+ T cells were incubated with autologous B cells (25,000 cells, ratio 1:1) that were pulsed with the indicated peptides. Unpulsed B cells (medium) and B cells pulsed with CEF–MHC class I control peptide pool “plus” (CEF+) were used as negative and positive controls, respectively. Peptide IVRCIGVSL was tested in PBMCs from six individuals, and peptide RPRSQPSSL was tested in PBMCs from eight participants.

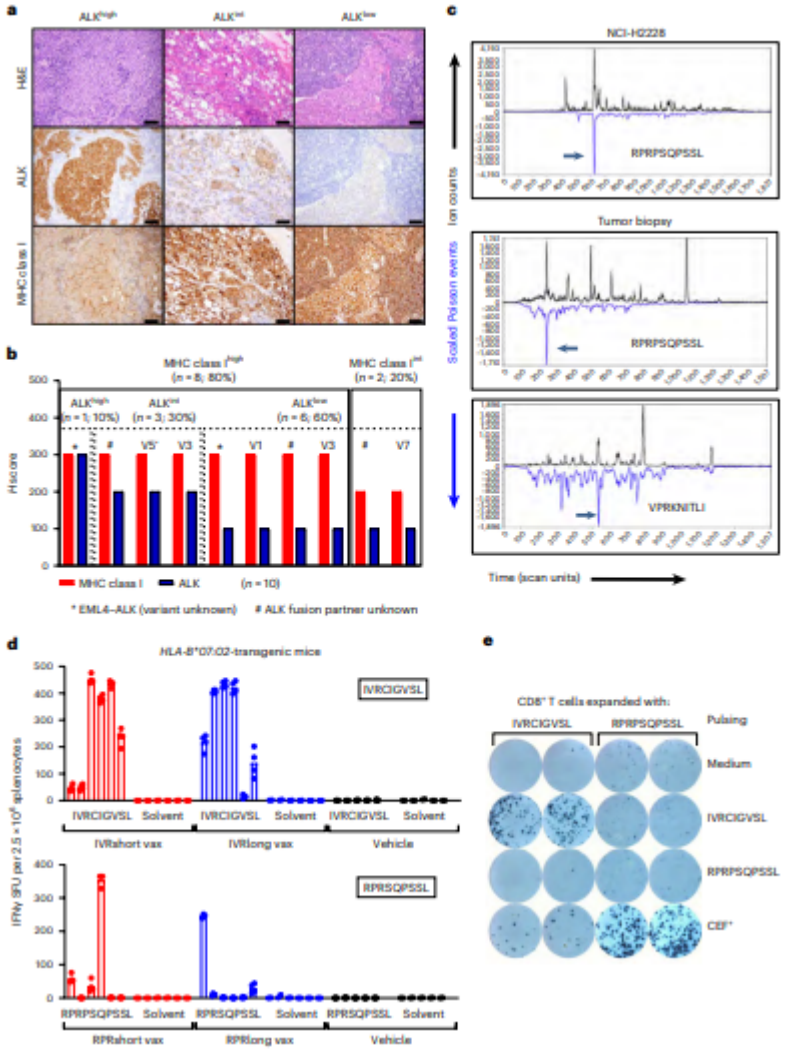

Fig. 8 | Lack of detectable toxicity of the ALK vaccine. a, Schematic representation of HLA-A*02:01- and HLA-B*07:02-transgenic mice vaccinated with either AMLDLLHVA or IVRCIGVSL peptides, respectively, and CDN adjuvant. b, Average mouse weight over time. Data are represented as mean ± s.e.m. (control, n = 6; HLA-A*02:01, n = 12; HLA-B*07:01, n = 12 mice). c, Representative H&E and pan-HLA immunohistochemistry staining of the hypothalamus region from HLA-A*02:01- and HLA-B*07:02-transgenic mice vaccinated as in a (×40 magnification); scale bars, 100 µm. d, Quantitative analysis of infiltrating CD8+ T cells per high-power field (HPF) in the hypothalamus region from HLAA*02:01-transgenic (n = 5) and HLA-B*07:02-transgenic (n = 5) mice vaccinated as in a. Naive mice (control, n = 4 mice) were used as negative controls. Data are represented as average number of four high-power fields per mouse (percent ± s.e.m.) and were analyzed by unpaired two-tailed Student's t-test (not significant, P = 0.1146 and P = 0.0703)

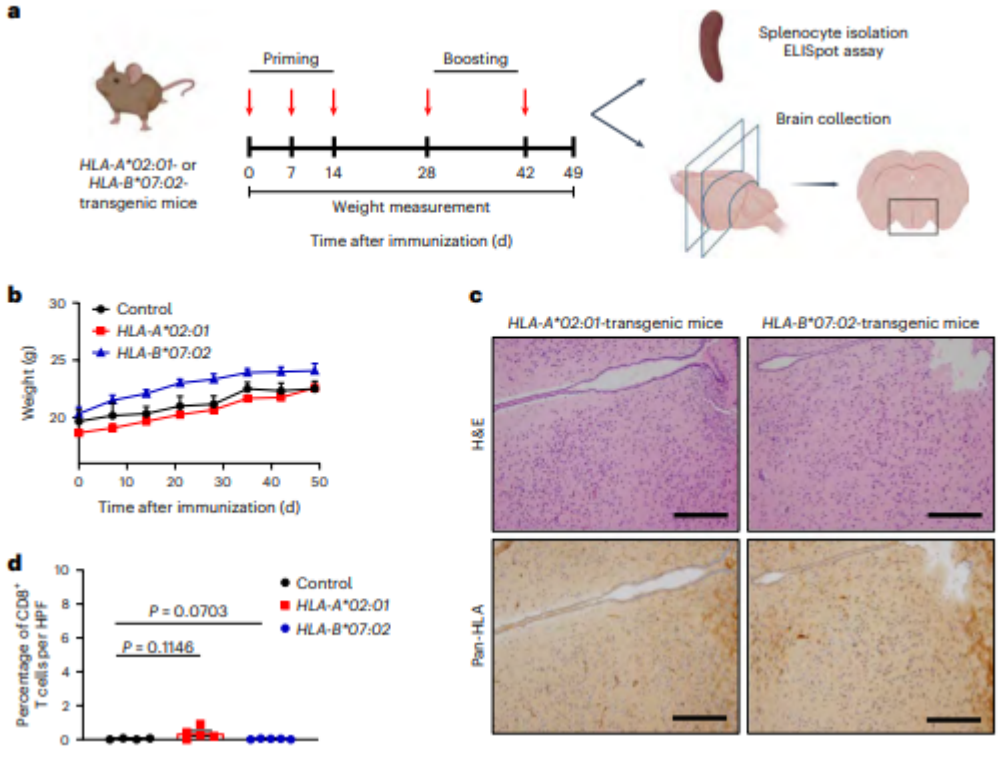
a
Priming
Boosting
0
7
14
28
42
49
Weight measurement
Time after immunization (d)
HLA-A*02:01- or HLA-B*07:02-transgenic mice
Splenocyte isolation
ELISpot assay
Brain collection
b
Control
HLA-A*02:01
HLA-B*07:02
Weight (g)
Time after immunization (d)
c
HLA-A*02:01-transgenic mice
HLA-B*07:02-transgenic mice
H&E
Pan-HLA
d
Control
HLA-A*02:01
HLA-B*07:02
P = 0.0703
P = 0.1146
Percentage of CD8+ T cells per HPF

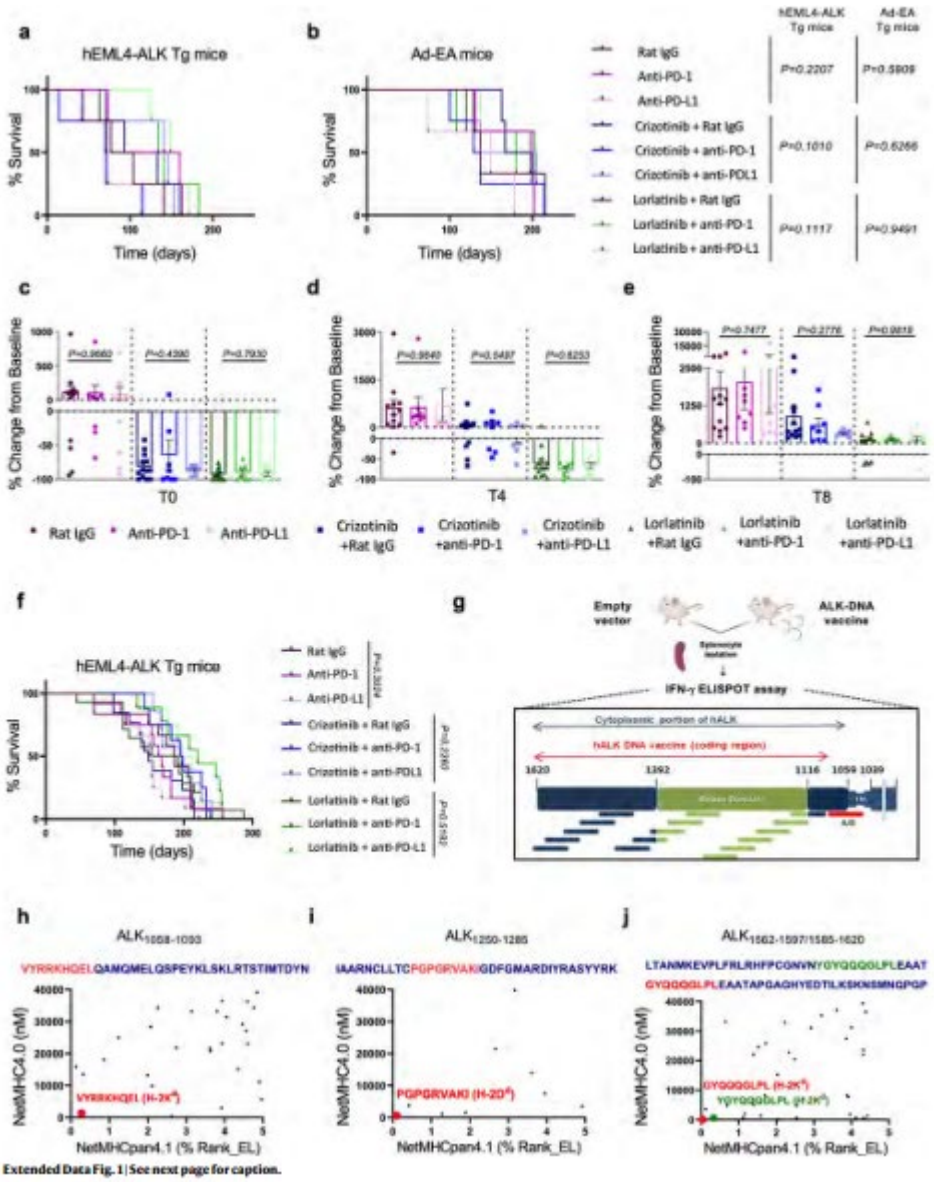

Extended Data Fig. 1 | See next page for caption.

Extended Data Fig. 1 | Immune checkpoint inhibitors (ICIs) do not increase the efficacy of ALK TKIs in ALK+ lung cancer mouse models.(a) Kaplan-Meier curves showing overall survival of mice described in Fig. 1c. Log-rank test, n/s, not significant (N = 3 mice per group). (b) Kaplan-Meier curves showing overall survival of mice described in Fig. 1d. Log-rank test; n/s, not significant (N = 4 mice per group) (c, d, e) Quantification of volume change compared with baseline tumor volume (change from baseline, % ± SEM) in hEML4-ALK Tg mice treated with higher doses (crizotinib: 100 mg/kg DIE; lorlatinib 10 mg/kg DIE) of ALK inhibitors and ICIs at T0 (c), T4 (d), and T8 (e) (Rat IgG, N = 12; anti-PD-1, N = 8; anti-PD-L1, N = 8; Crizotinib + Rat IgG, N = 13; Crizotinib + anti-PD-1, N = 8; Crizotinib + anti-PD-L1, N = 7; Lorlatinib + Rat IgG, N = 14; Lorlatinib + anti-PD-1, N = 7; Lorlatinib + anti-PD-L1, N = 8 mice). P values were calculated using an ordinary one-way Anova. (f) Kaplan-Meier curves showing overall survival

of hEML4-ALK Tg mice treated with higher doses of ALK inhibitors and ICIs. Logrank test; P values not significant. (Rat IgG, N = 12; anti-PD-1, N = 12; anti-PD-L1, N = 12; Crizotinib + Rat IgG, N = 13; Crizotinib + anti-PD-1, N = 8; Crizotinib + anti-PD-L1, N = 7; Lorlatinib + Rat IgG, N = 14; Lorlatinib + anti-PD-1, N = 9; Lorlatinib + anti-PD-L1, N = 8 mice). (g) Schematic representation of ALK peptide screening. Mice were vaccinated with a DNA encompassing the cytoplasmic portion of ALK, as previously described29. A set of 21 synthetic long peptides (SLPs) encompassing the coding region of the ALK-DNA vaccine was synthesized. Peptides A/B were synthetized to cover the cytoplasmic portion of hALK protein that is not represented in the ALK-DNA vaccine. (h-j) Benchmarking MHC-I algorithms for peptide-binding affinity prediction. NetMHC4.0 showing peptide affinity (predicted IC50 values in nM) vs. NetMHCpan4.1 showing the rank of the elution ligand likelihood (%Rank_EL). Computational predictions of peptide binding to MHC-I of SLPA (h), SLP7 (i) and SLP20 and 21 (j). Each dot represents a peptide. Peptide sequences and their correspondent predicted MHC-I allele can be found in Supplementary Table 3. Peptides represented in red or green indicate the best binder candidates

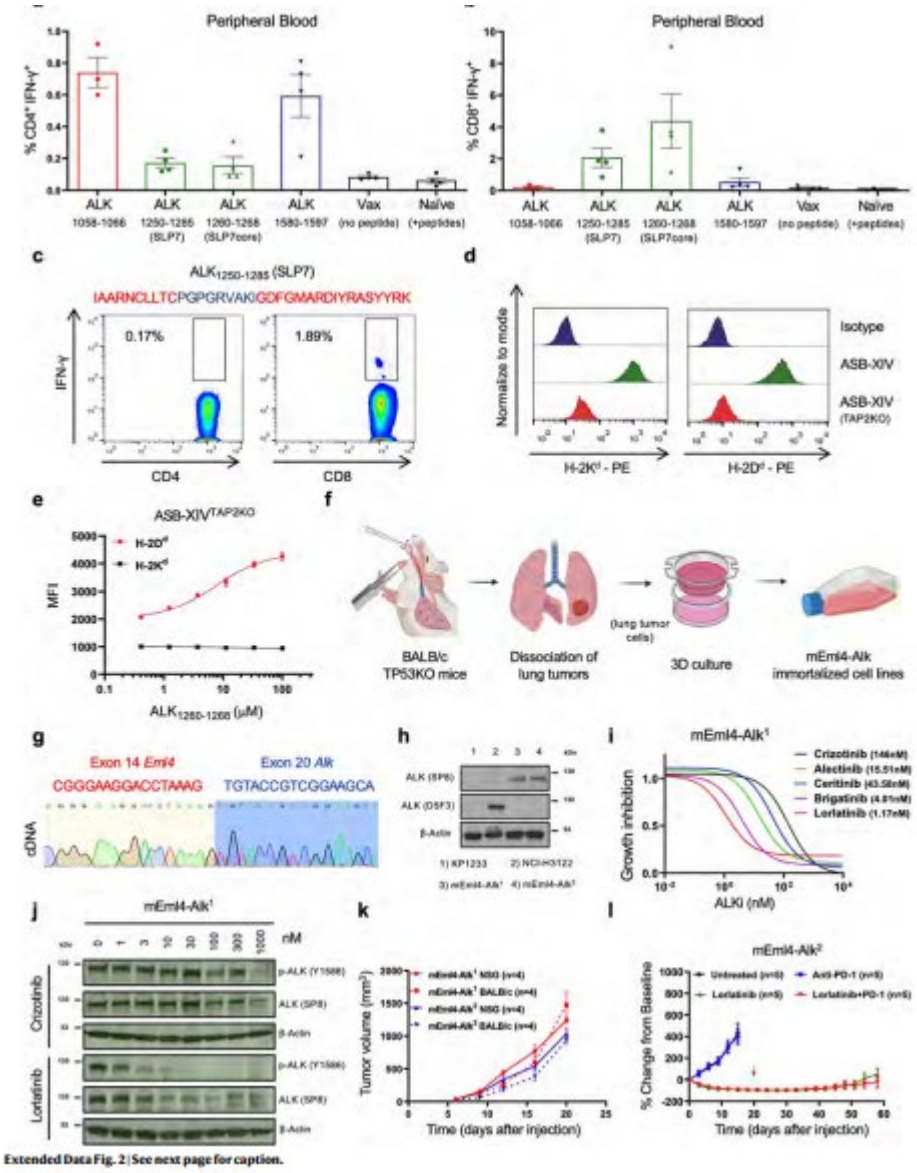

Extended Data Fig. 2 | See next page for caption.

Extended Data Fig. 2 | Identification of ALK immunogenic peptides in mouse models.(a, b) IFN-γ intracellular staining of CD4+ -gated (a) and CD8+ - gated (b) peripheral mononuclear cells (PBMCs) isolated from mice vaccinated with the indicated peptides and stimulated in vitro with the same peptide (%± SEM). Each dot represents a mouse (ALK1058-1066, n = 3; remaining groups, N = 4 mice). (c) IFN-γ intracellular staining in CD4+ and CD8+ splenocytes isolated from a representative mouse (N = 3 independent mice) vaccinated with SLP7 and pulsed with 10 μg/mL of the same peptide. (d) Representative flow cytometric analysis of H-2Kd and H-2Dd expression on ASB-XIV and ASB-XIVTAP2KO cells. Experiment performed three times. (e) H-2Dd and H-2Kd staining of ASB XIVTAP2KO cells incubated with increasing concentrations of PGPGRVAKI peptide displayed as mean fluorescence intensity (MFI) (± SEM) (n = 3 independent experiments). (f) Schematic representation of the generation of the mEml4- Alk immortalized cell lines. (g) Sanger sequencing chromatogram showing the mElm4-Alk inversion. The mouse Eml4-Alk inversion involves exon 14 of Eml4 and exon 20 of mouse Alk. (h) Representative immunoblot analysis (N = 3 independent experiments with

similar results) showing mEML4-ALK protein expression in two mEml4-Alk (mEml4-Alk1 and mEml4-Alk2) immortalized cell lines. The K-RasG12D KP1233 cell line was used as a negative control; ALK SP8 antibody recognizes the murine EML4-ALK (arrow); ALK D5F3 antibody recognizes the human EML4-ALK in NCI-H3122. *Indicates a non-specific band recognized by the SP8 antibody. (i) Dose response curves of mElm4-Alk1 cells to different ALK TKIs (crizotinib, N = 2 independent experiments; alectinib, N = 1; ceritinib, N = 1; brigatinib, N = 2 independent experiments; and lorlatinib, N = 2 independent experiments). (j) Representative immunoblot for the indicated proteins in mEml4-Alk1 cells treated with crizotinib and lorlatinib at the indicated concentrations for 6 h (N = 2 independent experiments with similar results). (k) Subcutaneous tumor growth (mm3 ± SEM) of mEml4-Alk-1 and mEml4-Alk-2 immortalized cell lines in NSG and syngeneic BALB/c mice (N = 4 mice per group). (l) Quantification of volume changes compared with baseline tumor volume (change from baseline, % ± SEM) in syngeneic BALB/c mice injected subcutaneously with a mEml4-Alk cell line and treated as indicated. Red arrow indicates the end of treatment (N = 5 mice per group)

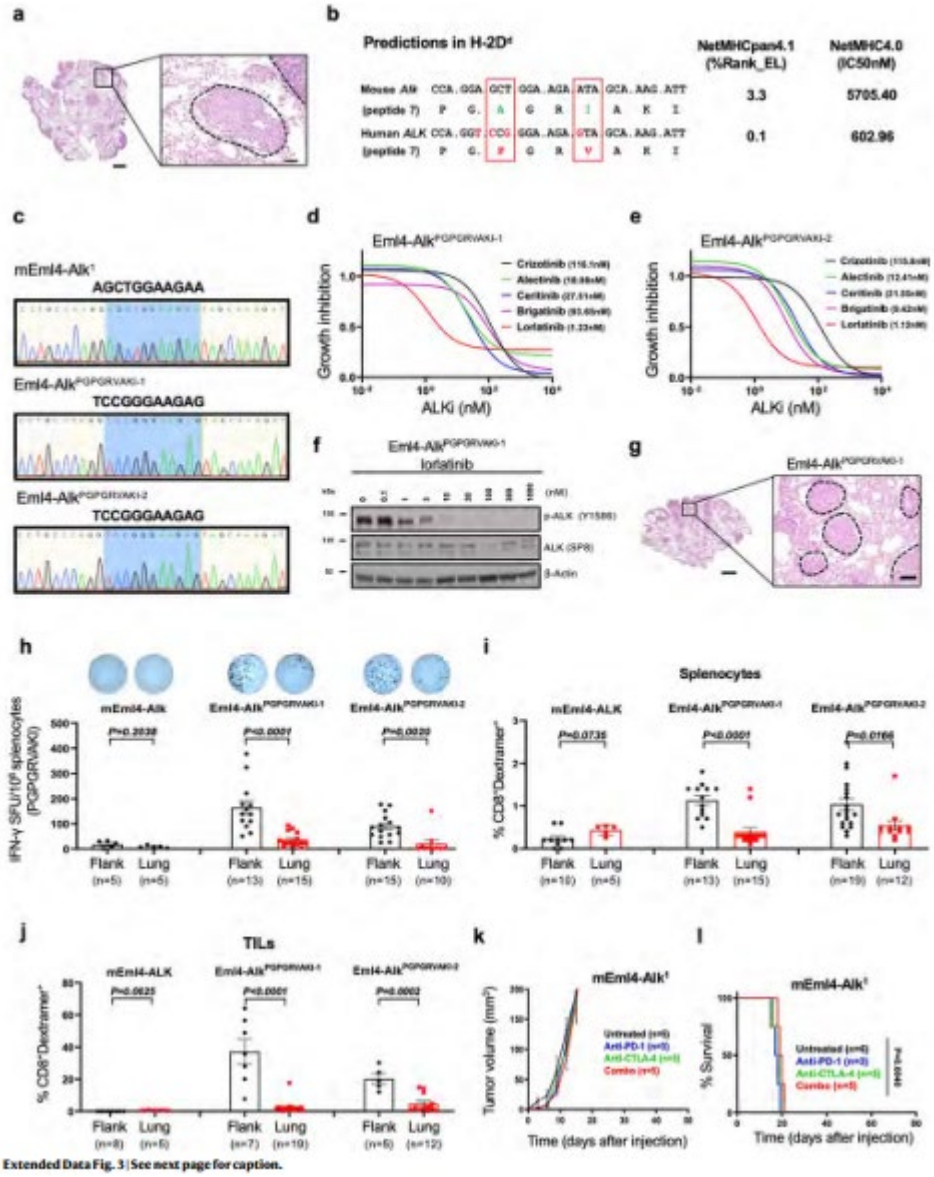

Extended Data Fig. 3 | See next page for caption.

Extended Data Fig. 3 | Generation and immunogenicity of Eml4-AlkPGPGRVAKI immortalized cell lines.(a) Representative H&E image of lung tumors generated in syngeneic BALB/c mice injected intravenously with mEml4-Alk. 2x magnification (left panel); 40x magnification (right panel) (n = 3 independent mice). Scale bar left = 1.5 mm; Scale bar right= 100 µm. (b) Schematic illustration of mouse and human ALK short peptide 7 sequences differences and CRISPR/ Cas9-edited DNA bases (Red). NetMHC4.0 showing peptide affinity (predicted IC50 values in nM) for H-2Dd and NetMHCpan4.1 showing the rank of the elution ligand likelihood (%Rank_EL) for H-2Dd . (c) Sanger sequencing chromatogram showing the cDNA sequence of mEml4-Alk (upper panel), Eml4-AlkPGPGRVAKI-1 (middle panel), and Eml4-AlkPGPGRVAKI-2 (lower panel) of PGPGRVAKI peptide. (d,e) Dose response curves of Eml4-AlkPGPGRVAKI-1 (d) and Eml4-AlkPGPGRVAKI-2 (e) cell lines to different ALK inhibitors (crizotinib, alectinib,

ceritinib, brigatinib, and lorlatinib). Two independent experiments were performed for each ALK inhibitor in each cell line. (f) Representative immunoblot for the indicated proteins in Eml4-AlkPGPGRVAKI-1 cells treated with lorlatinib at the indicated concentrations for 6 h (N = 2 independent experiments with similar results). (g) Representative H&E of lung tumors generated in syngeneic BALB/c mice injected intravenously with Eml4-AlkPGPGRVAKI-1. 2x magnification (left panel); 40x magnification (right panel) (n = 3 independent mice). Scale bar left = 1.5 mm; Scale bar right= 100 μm. (h) IFNγ-ELISPOT analysis of freshly isolated splenocytes from tumor-bearing BALB/c mice 15 days after been injected either subcutaneously (flank) or intravenously (lung) with mEml4-Alk (left panel), Eml4-AlkPGPGRVAKI-1 (middle panel), and Eml4-AlkPGPGRVAKI-2 (right panel) cells. Data is shown as average number of spot forming units (SFU ± SEM). Unpaired two-tailed Student's t test, not significant, P = 0.2038; **P

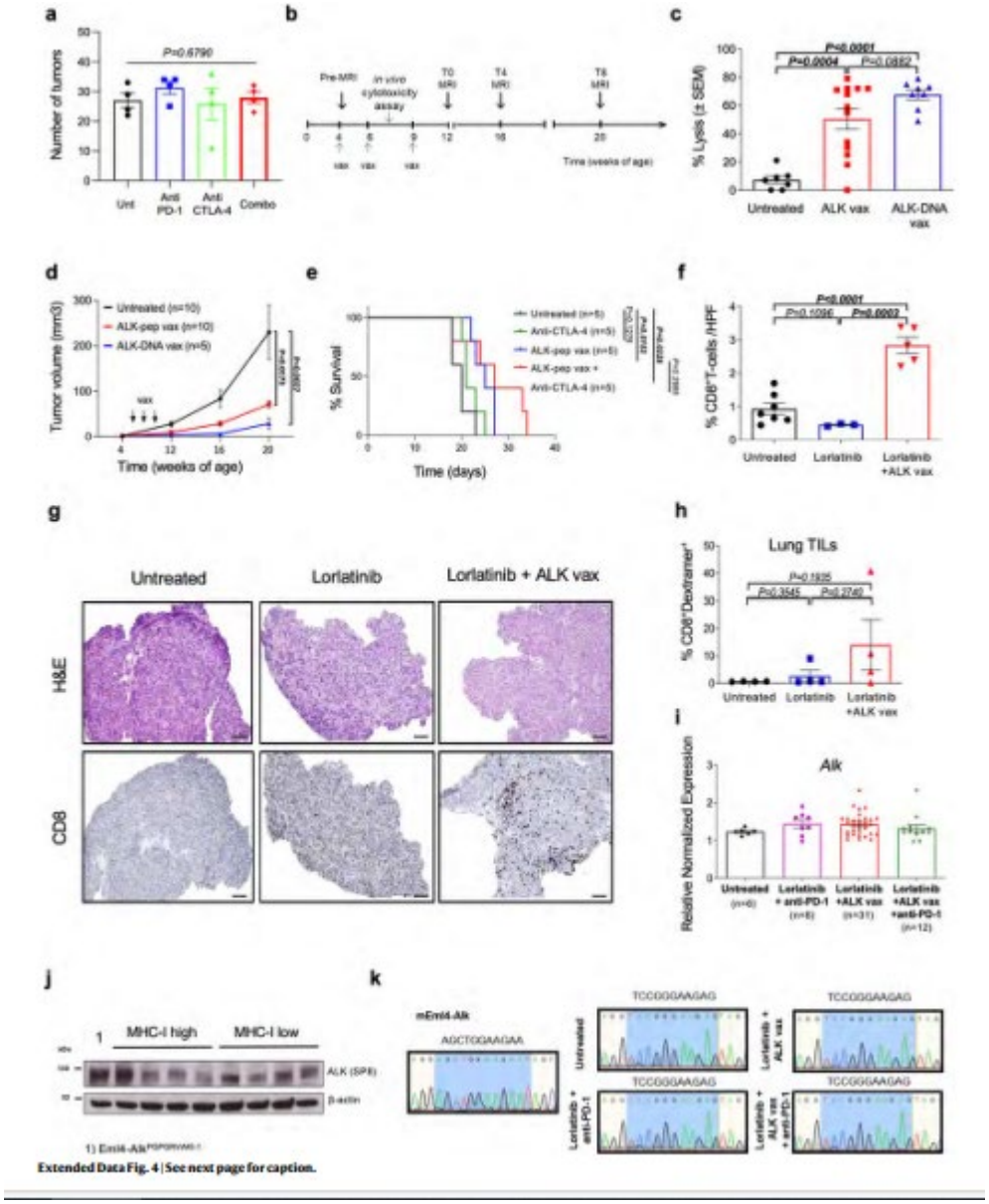

Extended Data Fig. 4 | See next page for caption.

Extended Data Fig. 4 | Immunogenicity of the ALK vaccine in mice.(a) Quantification of the number of tumors counted on a histology section taken in the middle of the lungs from mice shown in Fig. 3g. Each dot represents an individual mouse (n = 4 biological independent mice per group). Data are represented as mean ± SEM. Unpaired two-tailed Student's t test, not significant, P = 0.6790). (b) Schematic representation of treatment protocol of hEML4-ALK Tg mice vaccinated with either an ALK DNA vaccine29 or an ALK amph-vaccine63. (c)In vivo cytotoxic activity represented as % of lysis of target ALK+ cells (± SEM) by ALK-specific CD8+ T-cells in mice treated as in b. Each dot represents a mouse (Untreated, N = 7; ALK vax, N = 13, ALK-DNA vax, N = 8 mice). Unpaired two-tailed Student's t test, not significant, P = 0.0882; ***P = 0.0004; ****P

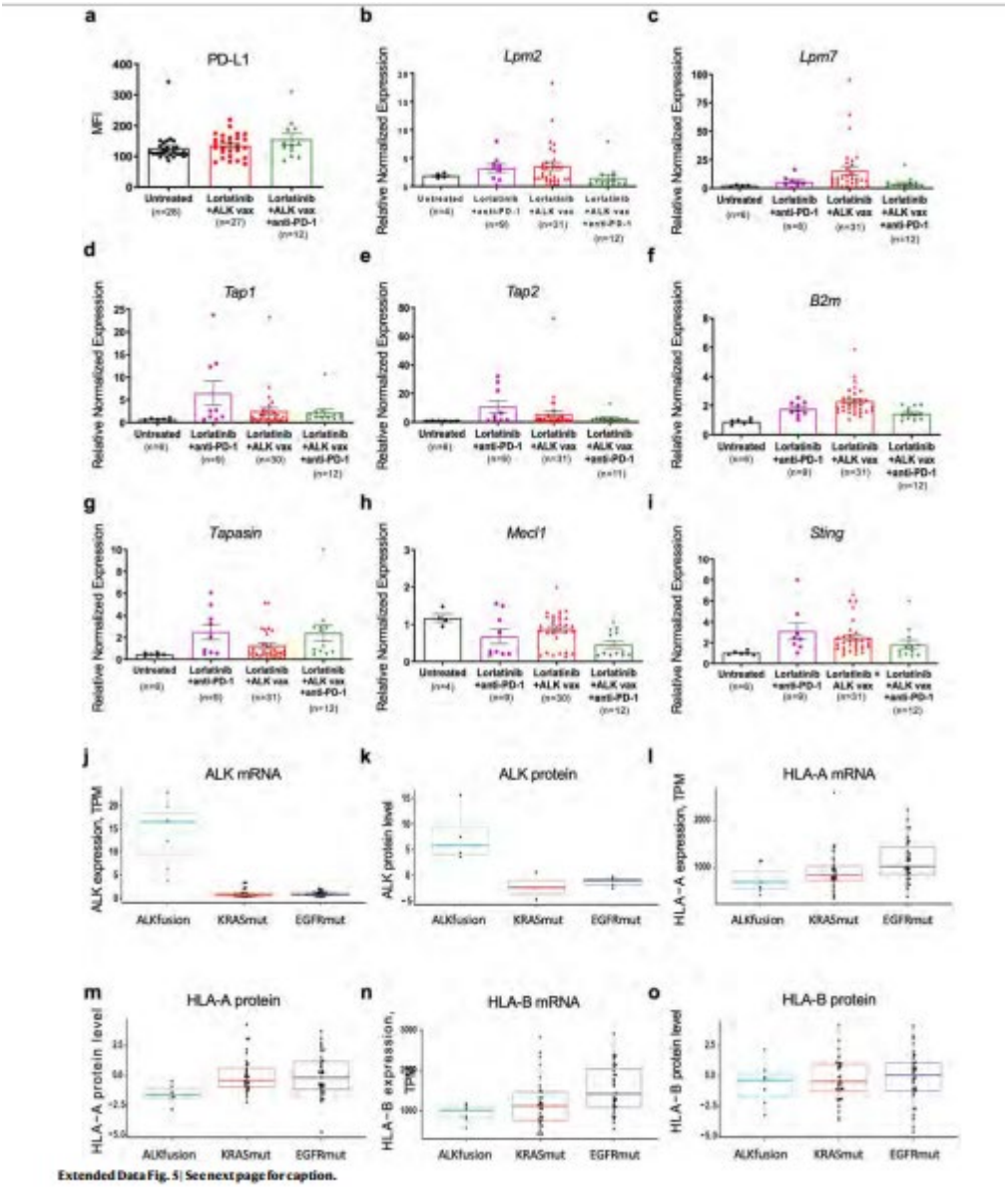

Extended Data Fig. 5 | See next page for caption.

Extended Data Fig. 5 | Characterization of tumors that escaped the ALK vaccine and MHC-I expression in human ALK + NSCLC.(a) PD-L1 expression of cell lines isolated from lung tumors that escaped the indicated treatment, displayed as mean fluorescence intensity (MFI) (± SEM). Each dot represents an individual tumor. (b-i) Relative normalized mRNA expression of Lpm2(b), Lpm7(c), Tap1(d), Tap2(e), B2m (f), Tapasin(g), Mecl1 (h), and Sting (i) genes in tumor lines isolated ex vivo from lung tumors that escaped the indicated treatments. For all samples the values were normalized to the expression levels of the parental Eml4-AlkPGPGRVAKI-1 cell line cultivated in vitro (± SEM). The N shown on the figure corresponds to

the number of ex vivo cell lines isolated and analyzed per group. (j-o) ALK+ NSCLC expresses HLA-A/B mRNA and protein at levels comparable to NSCLC with other oncogenic drivers (CPTAC dataset). Boxplot showing mRNA and protein expression of ALK (j, k), HLA-A (l,m), HLA-B (n, o), from cases of ALK+ NSCLC from the Clinical Proteomic Tumor Analysis Consortium (CPTAC)44. Fusion variants of the 7 ALK + NSCLC cases: 5 EML4-ALK, 1 ANKRD36B-ALK, 1 HMBOX1-ALK. Number of samples with ALK-fusion: n = 7, KRAS-mutation: n = 32, EGFR-mutation: n = 35, wild type samples not represented on the plot: n = 36. The boxplots show the median (line), and the interquartile range (IQR), and the whiskers represent 1.5× the IQR ± the upper and lower quartiles, respectively

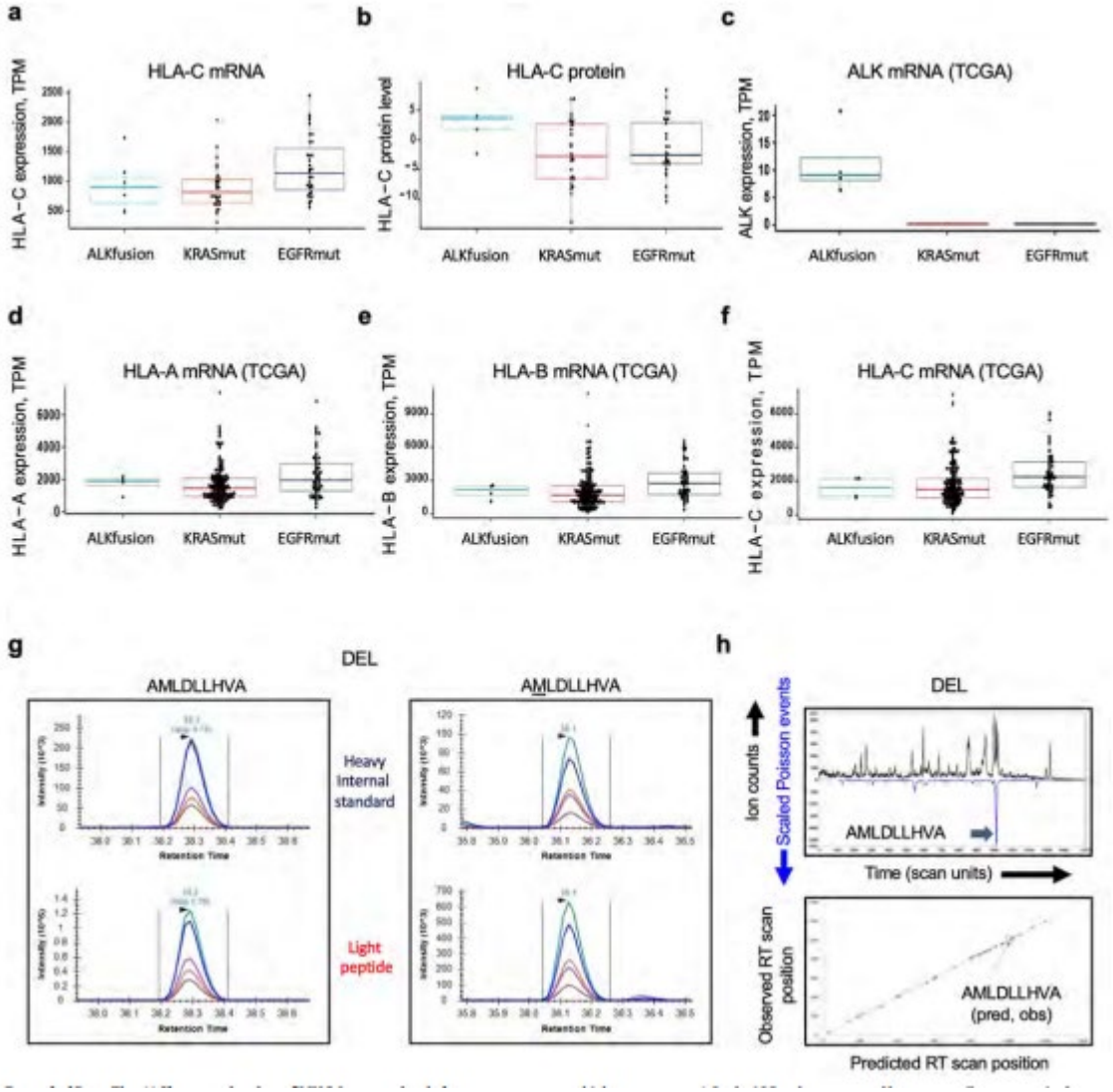

Extended Data Fig. 6 | Characterization of MHC-I expression in human ALK + NSCLC and identification of MHC-I human ALK peptides in human ALK+ lymphoma cell lines.(a-b) Boxplot showing mRNA and protein expression of HLA-BC from cases of ALK+ NSCLC from the Clinical Proteomic Tumor Analysis Consortium (CPTAC)44. (c-f) ALK+ NSCLC express HLA-A/B/C mRNA and protein at levels comparable to NSCLC with other oncogenic drivers (TCGA dataset). Boxplot showing mRNA expression of ALK (c), HLA-A (d), HLA-B (e), and HLA-C (f) from cases of ALK+ NSCLC from The Cancer Genome Atlas (TCGA) LUAD gene expression (http://cancergenome.nih.gov). All 4 ALK+ NSCLC had an EML4-ALK fusion. Number of samples with ALK-fusion: n = 4, KRAS-mutation: n = 155, EGFR-mutation: n = 56, wild type samples not represented on the plot: n = 301. The boxplots show the median (line), and the interquartile range (IQR), and the whiskers represent 1.5× the IQR ± the upper and lower quartiles, respectively. (g) Targeted mass spectrometry from HLA A*02:01 immunoprecipitations of the ALCL cell line DEL. Oxidized and non-oxidized methionine forms of the peptide AMLDLLHVA were monitored. (h) Poisson LC-DIAMS plots from pan-HLA immunoprecipitations of the ALK+ ALCL cell lines DEL. Poisson plots combine an extracted ion chromatogram (XIC) for the peptides' precursor m/z (black trace) with an inverted, scaled Poisson chromatogram (blue trace, see Methods). Peptide detection (see Methods) at an elution point is associated with coincident precursor and Poisson peaks, here marked by blue arrows The elution position lies near the predicted elution position determined by a retention time peptide set added to the DEL (h, lower panel) samples and, after sample data was collected, the synthetic set of ALK peptides.

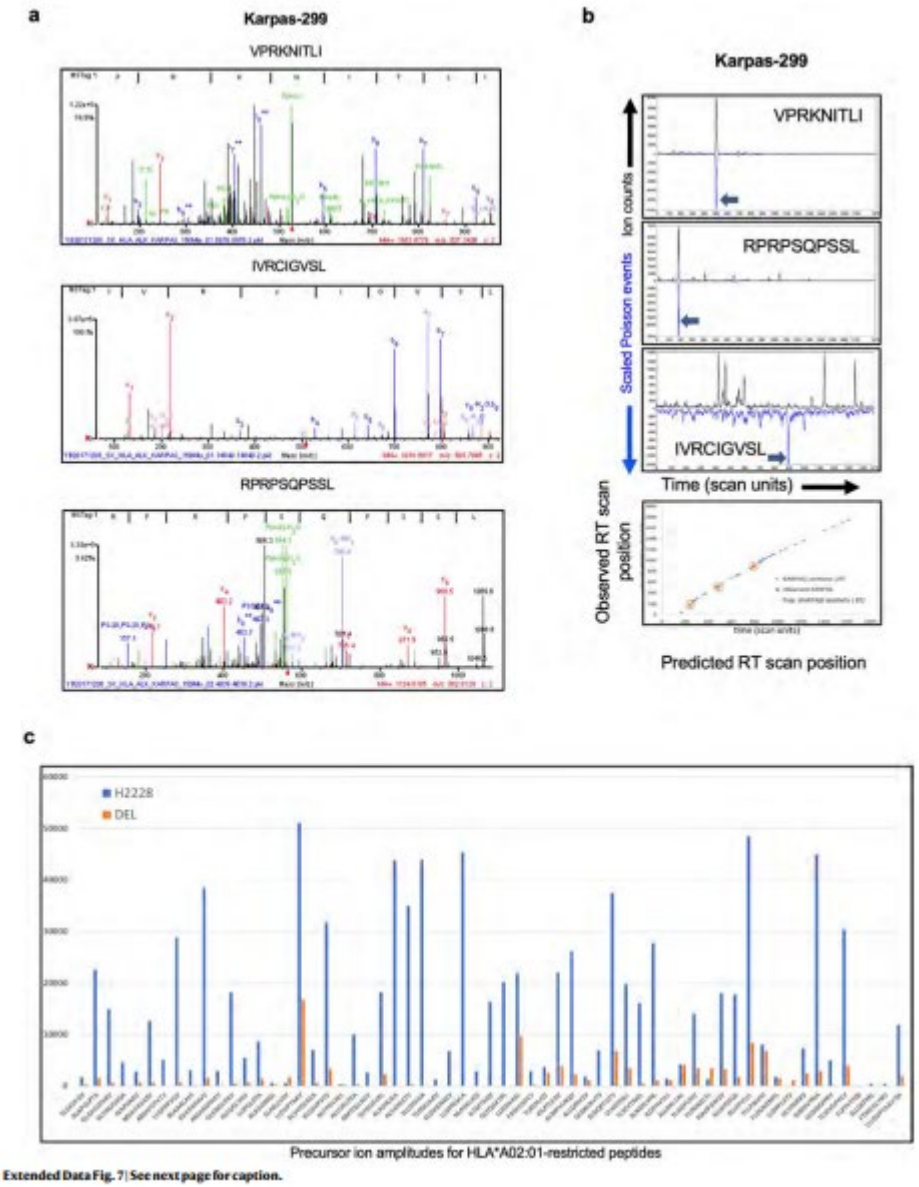

Extended Data Fig. 7 | See next page for caption.

Extended Data Fig. 7 | Identification of MHC-I human ALK peptides in human ALK+ cell lines.(a) Identification of ALK-specific peptides by discovery mass spectrometry from pan-HLA immunoprecipitations of the ALCL cell line Karpas-299. (b) Poisson LC-DIAMS plots from pan-HLA immunoprecipitations of the ALK+ ALCL cell lines Karpas-299. Poisson plots combine an extracted ion chromatogram (XIC) for the peptides' precursor m/z (black trace) with an inverted, scaled Poisson chromatogram (blue trace, see Methods). Peptide detection (see Methods) at an elution point is associated with coincident precursor and Poisson peaks, here marked by blue arrows The elution position lies near the predicted elution position determined by a retention time peptide set added to the Karpas-299 (b, lower panel) samples and, after sample data was collected, the synthetic set of ALK peptides. (c) Poisson analysis of the same LC-DIAMS datasets detecting AMLDLLHVA in DEL but not in NCI-H2228, using reference information for a set of common HLA-A*02:01 peptides, identifies substantially better A02:01 peptide recovery from NCI-H2228. Hence, that NCI-H2228 cells do not present HLA-A*02:01 peptides from ALK, including the strong binding AMLDLLHVA peptide detected

in the ALCL cell line DEL, cannot be associated with poor overall recovery of A*02:01 peptides.

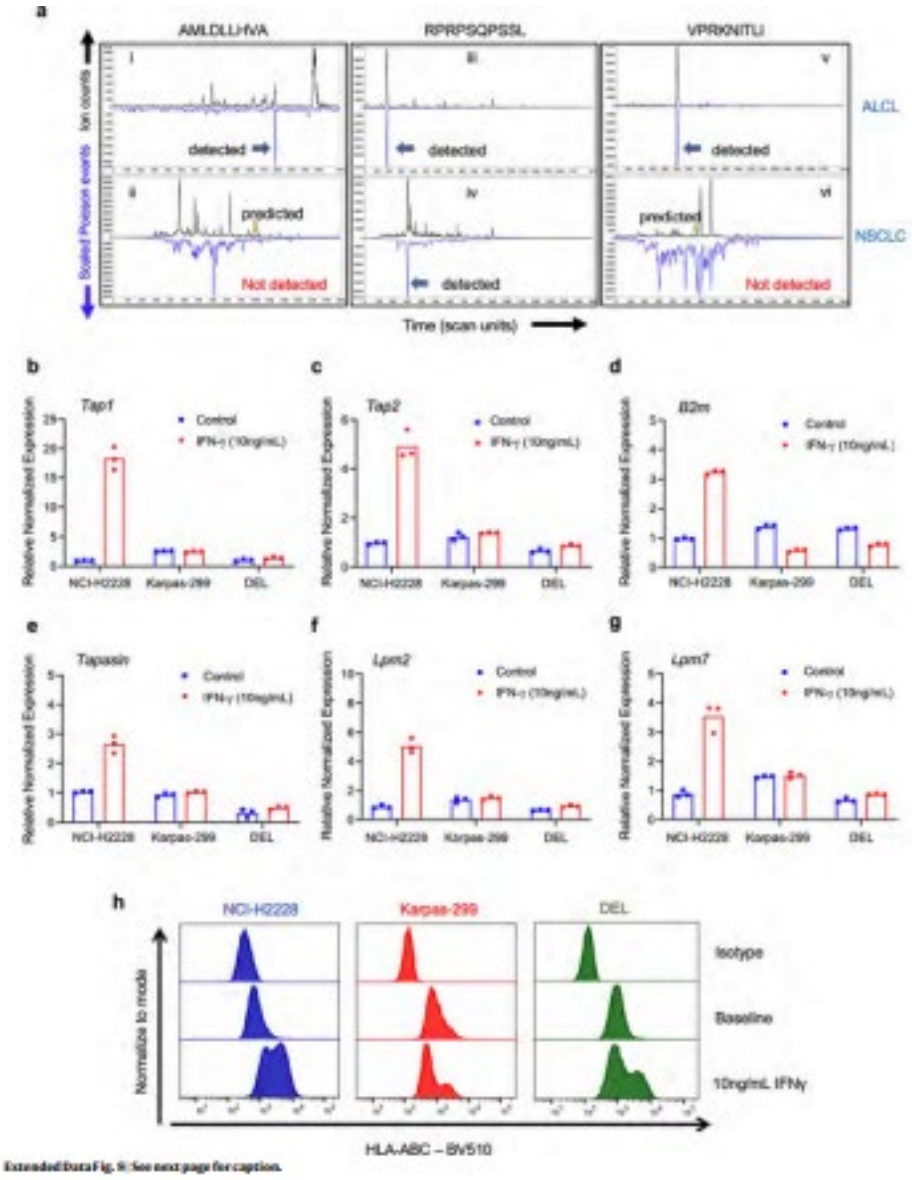

Extended Data Fig. 8 | Identification of MHC-I human ALK peptides and characterization of the immunoproteasome in human ALK+ cell lines. (a) Cell type specificity in antigen presentation. HLA A*02:01 restricted ALK peptide AMLDLLHVA is displayed in DEL cells (i) but not in H2228 cells (ii). These lines are HLA A*02:01 positive and an abundant display of common HLA-A2 peptides was detected. Both HLA B*07:02 restricted ALK peptides RPRPSQPSSL and VPRKNITLI are displayed in Karpas-299 cells (iii and v) while RPRPSQPSSL is displayed in H2228 cells (iv) and VPRKNITLI is not (vi). Blue arrows mark detection signatures associated with coincident XIC and Poisson peaks. For the negative detections in (ii) and (vi) orange arrows mark the expected elution position as calculated from the elution of added retention

time peptides (see Methods). Expected elution positions and detection positions overlap for positive detection, as is the case for the other 4 panels. (b-g) Expression of Tap1, Tap2, B2M, Tapasin, Lmp2 and Lmp7 in ALK+ lung cancer and lymphoma cell lines. Relative normalized mRNA expression of (b)Tap1, (c)Tap2, (d)B2m, (e) Tapasin, (f) Lpm2, (g) Lpm7 genes in NCI-H2228, Karpas-299 and DEL cell lines either at baseline or stimulated for 24 hours with 10 ng/mL IFN-γ. Values are normalized to the expression levels of NCI-H2228 line at baseline. Dots represent technical replicates from a single experiment. (h) Expression of HLA molecules was determined by flow cytometry with a pan-HLA antibody in NCI-H2228, Karpas-299 and DEL cell lines either at baseline or stimulated for 24 hours with 10 ng/mL IFN-γ.

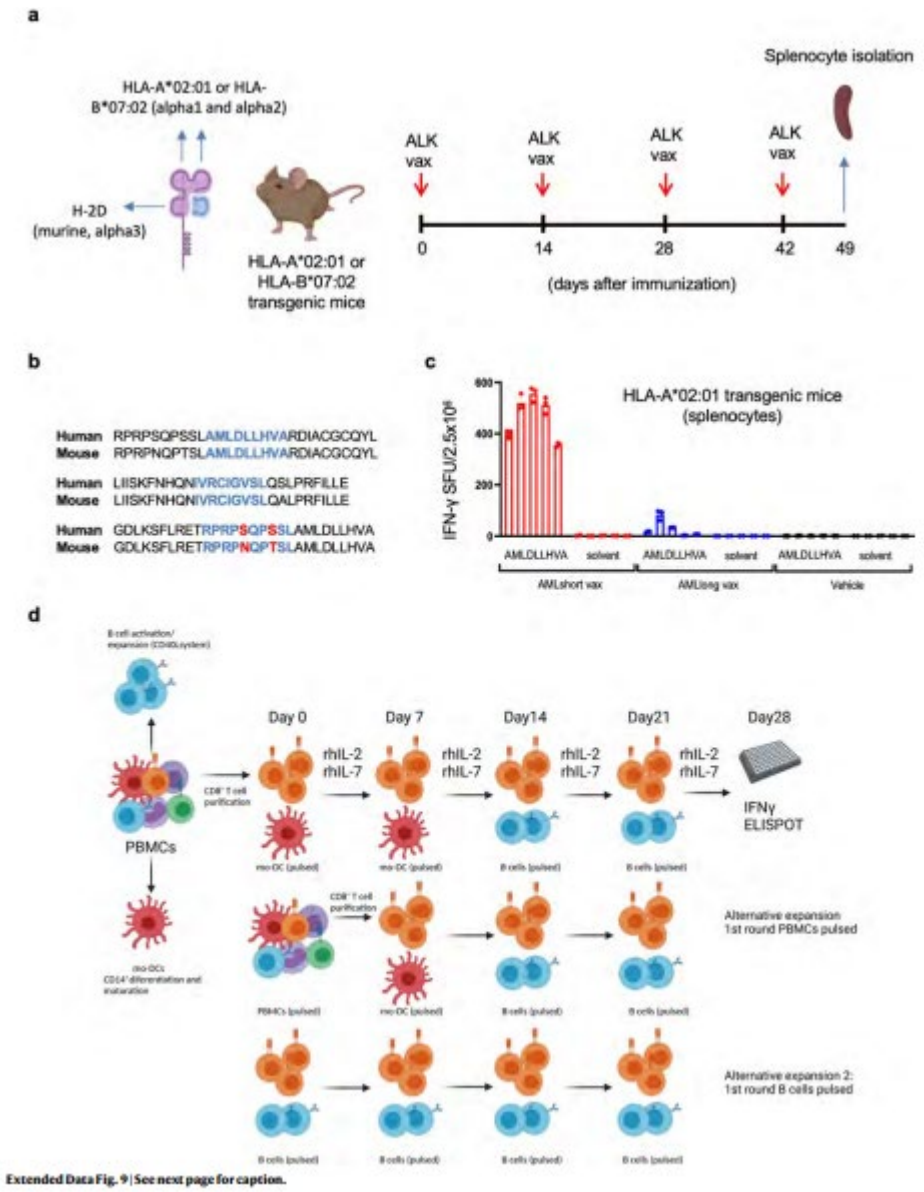

Extended Data Fig. 9 | See next page for caption.

Extended Data Fig. 9 | Immunogenicity of ALK-specific peptides in HLA transgenic mice.(a) Scheme of vaccination of HLA-A*02:01 and HLA-B*07:02 transgenic mice. (b) Sequence comparison of the ALK peptides between mouse and human. (c) Quantification of IFN-γ

ELISPOT assays of splenocytes isolated from HLA-A*02:01 transgenic mice vaccinated with AMLshort or AMLlong peptides with CDN adjuvant. PBS was used as a vaccination control (N = 5 mice per group). Each bar represents spot forming units (SFU) from splenocytes isolated from an individual mouse and incubated with either peptide AMLDLLHV or peptide solvent (DMSO) as a negative control. Two independent experiments were performed. Data are represented as three technical replicates from one experiment. (d) Schematic representation of the expansion protocol for human CD8+ T cells from PBMCs of patients with NSCLC in the presence of ALK-specific peptides. The displayed alternative expansion methods were applied for those patients with lower amount of PBMCs available

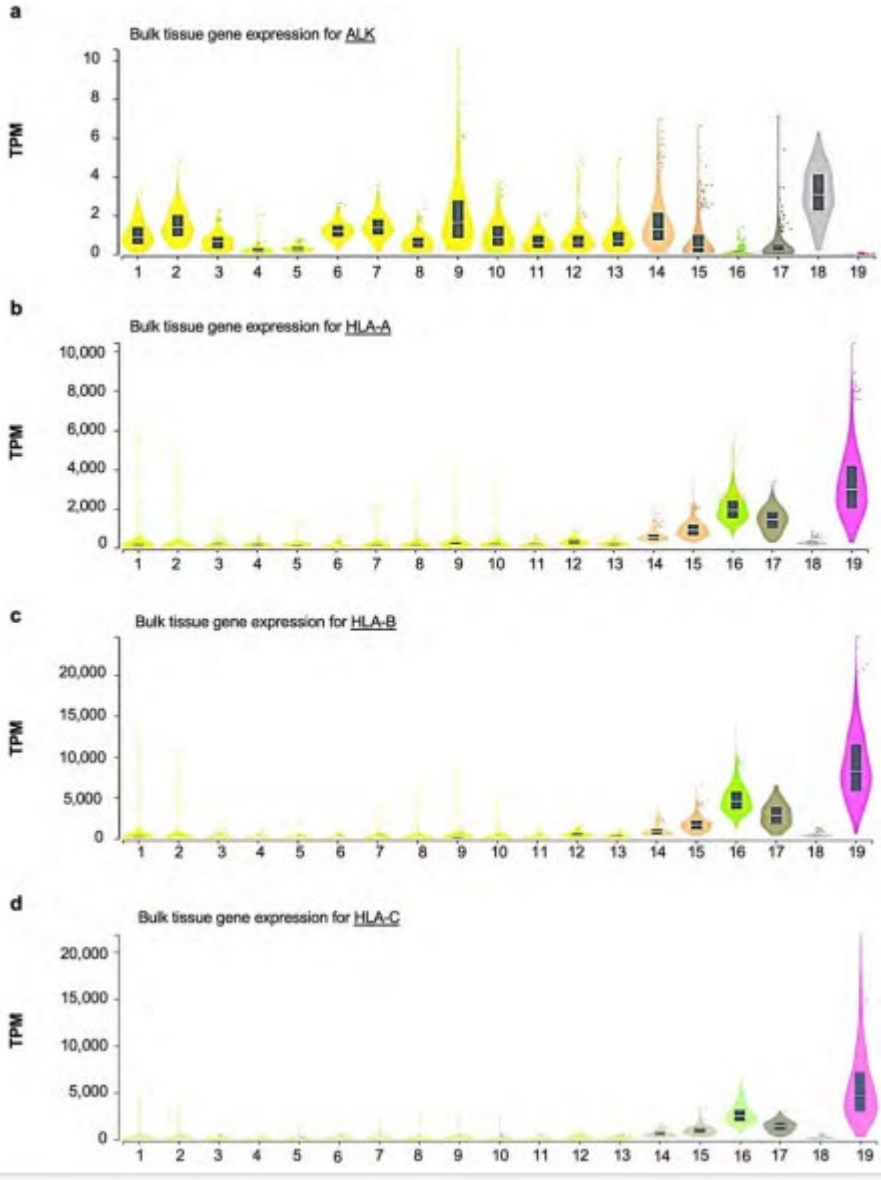

Extended Data Fig. 10 | Physiologic ALK expression is low and limited to certain areas in the brain with low expression of HLA-A, HLA-B and HLA-C. ALK (a), HLA-A (b), HLA-B (c) and HLA-C (d) mRNA expression in the indicated tissues according to the Genotype-Tissue Expression (GTEx) project (https:// gtexportal.org/home/). 1) Amygdala (n = 152); 2) Anterior cingulate

cortex (BA24) (n = 176); 3) Caudate (basal ganglia) (n = 246); 4) Cerebellar Hemisphere (n = 215); 5) Cerebellum (n = 241); 6) Cortex (n = 255); 7) Frontal Cortex (BA9) (n = 209); 8) Hippocampus (n = 197); 9) Hypothalamus (n = 202); 10) Nucleus accumbens (basal ganglia) (n = 246); 11) Putamen (basal ganglia) (n = 205); 12) Spinal cord (cervical c-1) (n = 159); 13) Substantia nigra (n = 139); 14) Colon – Sigmoid (n = 373); 15) Colon – Transverse (n = 406); 16) Lung (n = 578); 17) Small Intestine - Terminal Ileum (n = 187); 18) Testis (n = 361); 19) Whole Blood (n = 755). The line inside each box is the median, upper box border represents the 75th quartile, lower box border represents the 25th quartile and whiskers represent the range.